Hygro-mechanical response of oak wood cabinet door panels under relative humidity fluctuations

Heritage Science

RESEARCH ARTICLE

Open Access

CrossMark

Hygro-mechanical response of oak wood cabinet door panels under relative humidity fluctuations

R. A. Luimes[1], A. S. J. Suiker[1*], A. J. M. Jorissen[1], P. H. J. C. van Duin[2] and H. L. Schellen[1]

Abstract

Indoor climate fluctuations are regarded as one of the major risks for the emergence of damage in historical works of art. For a safe preservation of their art objects museums try to minimize this risk, which is typically done by imposing strict limitations on the indoor temperature and humidity conditions. The high energy demand resulting from this approach, however, undermines the aim of preeminent museums to execute a sustainable preservation strategy of their collections. A rational improvement of this aspect asks for detailed information on the history of museum objects, complemented by a thorough comprehension of the failure and deformation behaviour of museum objects under indoor climate fluctuations. Accordingly, in this paper the hygro-mechanical response of mock-ups of historical Dutch cabinet door panels made of oak wood is examined under several relative humidity variations. In specific, the mock-ups were subjected to (i) an instantaneous decrease of 40% relative humidity, (ii) eight successive, instantaneous drops of 5% relative humidity, and (iii) a varying relative humidity profile ranging between 35 and 71%. The shrinkage characteristics of mock-ups are translated to their damage susceptibility using an analytical hygro-mechanical bi-layer model. This model shows that restrained hygral shrinkage may originate from: (i) a difference in moisture content across the thickness direction of the panel, or (ii) a directional difference in the coefficient of hygroscopic expansions of structural components forming a coherent connection. The first type of shrinkage occurs in the outer regions of the panel thickness, while the second type of shrinkage takes place at the cleated ends. Further, by accounting for the age-dependency of the fracture strength of oak wood, a clear distinction can be made between the damage susceptibility of new door panels and historical door panels present in museum cabinets. The six main conclusions of the experimental study—conveniently summarized at the end of this paper—provide a scientific basis for the understanding of shrinkage cracks and dimensional changes observed on decorated oak wooden panels in historical Dutch cabinets, and thus may assist in advising museums on future sustainable preservation strategies and rational guidelines for indoor climate specifications.

Keywords: Historical museum objects, Mock-ups, Restrained hygral shrinkage, Damage resistance, Sustainable preservation

*Correspondence: a.s.j.suiker@tue.nl
[1] Department of the Built Environment, Eindhoven University
of Technology, P.O. Box 513, 5600 MB Eindhoven, The Netherlands
Full list of author information is available at the end of the article

Luimes *et al. Herit Sci* (2018) 6:72

Page 2 of 23

Introduction

The protection and preservation of works of art is important, as these objects constitute a significant part of our cultural heritage. Museums are responsible for safely preserving works of art and making their collections accessible to the public. This task is challenging: Indoor climate fluctuations, often caused by the entering public, may induce undesirable deformations and damage in the displayed objects, and therefore form a major concern to conservators and curators. Since the late nineteenth century the environmental control of museums has developed substantially, which, from the 1970s until the end of the twentieth century, has led to the formulation of specific conditions for indoor temperature and relative humidity fluctuations [1, 2]. In order to prevent climate-induced damage of susceptible art objects, these environmental guidelines prescribe strict limitations on indoor climate conditions. This results in a low risk preservation of susceptible collections, at the expense of high energy demands and costs. Only since the beginning of the twenty-first century museums tend to strive for a more sustainable collection management, by exploring whether strict indoor climate conditions can be relaxed without introducing an unacceptable risk of damage. Within the conservation community, this approach has been intensively debated [3–8], whereby three distinct positions are taken [1], based on (i) precautionary safety, (ii) proven safety and (iii) pragmatic risk management. To support the debate and find consensus among the distinct positions on sustainable collection management, additional

scientific research on the origin of climate-induced damage of museum objects is of utmost importance [1, 9].

Recently, various research efforts aimed at understanding and improving preservation procedures for historical works of art. For example, the Furniture Conservation Department of the Rijksmuseum has carried out several challenging conservation treatments on cabinets on stands decorated with marquetry [10, 11]. During the late seventeenth century these cabinets were very popular in the Netherlands, because of the magnificent, decorative surface layers applied on the large flat doors, see Fig. 1. In 2010, the Rijksmuseum organized a masterclass in which 17 pairs of Dutch seventeenth-century cabinet doors were studied extensively [10]. Despite the variety in substrate structures and construction methods used, all doors showed shrinkage cracks, see Fig. 2, and some doors were slightly warped. Inspired by these observations, a combined experimental–numerical study was initiated regarding the influence of historical and current indoor climate variations within a castle on the risk of damage to historical wooden door panels, see [12]. From similar grounds, the behaviour of two historical wooden pianofortes under mechanical and hygral loading was analysed numerically in [13], providing detailed insight into the damage observed on these objects. The mechanical interactions between the poplar substrate and the frame of the Mona Lisa, painted by Leonardo da Vinci, were experimentally investigated in [14]. The hygro-mechanical performance of the painting was determined, from which an estimation could be

a Historical cabinet, Jan van Mekeren. Oak veneered with various wood species, door: h=110 cm, w=80 cm, t=3.5 cm. Amsterdam, circa 1695-1710. Amerongen Castle, Amerongen.

b Historical cabinet. Oak veneered with olive wood and cedar, h=212 cm, w=178 cm, d=62.5 cm. The Netherlands, circa 1680-1700. Rijksmuseum, Amsterdam, BK-1960-19.

c Historical cabinet. Oak veneered with rosewood, walnut, padauk, purpleheart, ebony, olive wood, holly and bone, h=227 cm, w=192 cm, d=65 cm. The Netherlands, circa 1680-1710. Rijksmuseum, Amsterdam, BK-NM-6073.

Fig. 1 A selection of Dutch cabinets on stands decorated with marquetry

Luimes *et al. Herit Sci*   (2018) 6:72

Page 3 of 23

a Close-up of historical cabinet door, Jan van Mekeren. Oak veneered with various wood species, door: h=110 cm, w=80 cm, t=3.5 cm. Amsterdam, circa 1695-1710. Amerongen Castle, Amerongen.

b Close-up of historical cabinet door panel. Oak veneered with rosewood, walnut, padauk, purpleheart, ebony, olive wood, holly and bone, h=221 cm, w=192 cm, d=63 cm. The Netherlands, circa 1690-1710. Rijksmuseum, Amsterdam, BK-NM-6073.

Fig. 2 Shrinkage cracks (indicated by the white arrows) in the oak substrate

made of the appropriateness of the climate conditions applied in the exhibition room. The research reported in [15] focused on monitoring the dimensional response of an altarpiece located in a church in Italy, which made it possible to advise on the specific settings of the heating system used in the church. In [16–18], experimental tests were combined with numerical modelling to characterize the fatigue behaviour of mock-ups of single board panel paintings under sinusoidal, relative humidity fluctuations. In [19] mock-ups of panel paintings were subjected to step variations of the ambient relative humidity, in order to obtain detailed insight into their hygro-mechanical response.

In addition to research performed on specific objects, the ongoing debate within the conservation community regarding appropriate sustainable museum environments also revealed the need to provide the preservation of large museum collections with a firm, scientific basis [9, 20]. For this purpose, several long-term, multidisciplinary research projects were initiated, like the Managing Collection Environments Initiative by the Getty Conservation Institute [21], and the Climate4Wood project by the Eindhoven University of Technology, Delft University of Technology, Rijksmuseum and Cultural Heritage Agency of the Netherlands [22, 23]. The first project addresses compelling research questions related to the control and management of museum environments suitable for susceptible collections [21]. The response of hygroscopic materials and objects has been studied under climate fluctuations, and epidemiology [24] has been applied to susceptible objects in order to identify how the object condition or the adverse effect of the environment appears within large museum collections. In the second project the material properties,

indoor climate conditions, and type of construction of decorated oak wood panels present in the Rijksmuseum collection are investigated by combining an extensive museum study with advanced numerical modelling and dedicated laboratory and in-situ experiments [23]. From the museum study a large amount of data was collected in a systematic fashion; these data has been used (i) as input for experimental, numerical and in-situ studies on oak wood panels, and (ii) for constructing a reference case that can be employed for determining the condition of similar collections present in other museums. In addition, the possibility of a causal connection between the panel characteristics and the climate history of objects has been explored.

As part of the Climate4Wood project, in the present communication the hygro-mechanical response of mock-ups of historical Dutch cabinet door panels made of oak wood is examined experimentally under several relative humidity variations. More specifically, the mock-ups are subjected to (i) an instantaneous decrease of 40% relative humidity, (ii) 8 successive, instantaneous drops of 5% relative humidity, and (iii) a varying relative humidity profile ranging between 35 and 71%. The effect of the presence of cleated ends and veneer layers on restrained hygral shrinkage of the oak wood door panels is explored by distinguishing two basic types of shrinkage mechanisms. Further, the shrinkage response of the mock-ups is translated to their damage susceptibility using an analytical hygro-mechanical bi-layer model. In accordance with these research tasks, the paper is organized as follows. The "Experimental program" section discusses the experimental program, whereby the mock-ups, their preparation, the test set-up and the measurement scheme are described. The "Experimental results mock-ups A and

Luimes *et al. Herit Sci*   (2018) 6:72

Page 4 of 23

B" and the "Experimental results mock-ups C, D, E and F" sections treat the experimental results for the different mock-ups, analysing the time evolution of the panel deformations, the origin of restrained hygral shrinkage, and the risk of damage. Also, the development of the moisture profiles in the mock-ups is analysed. The six main conclusions of the experimental study are outlined in the "Conclusions" section.

Experimental program

The damage observed on door panels of historical Dutch cabinets is illustrated in Fig. 2, and, as reported in [10, 25], may be induced by indoor climate fluctuations. The present work aims at gaining more insight into this aspect, by performing an experimental program in which the deformation response and damage resistance of mock-ups of cabinet door panels under relative humidity fluctuations is analysed. Two mock-ups—referred to as mock-ups A and B—were subjected to a single decrease and multiple stepwise decreases in relative humidity, respectively, and four mock-ups—referred to as mock-ups C to F—were exposed to a varying relative humidity profile ranging between 35 and 71%. Mock-ups C to F also consider the influence of the presence of cleated ends and veneer layers on the panel response, as illustrated in Fig. 3.

Mock-ups

Historical Dutch cabinet doors typically consist of an oak wood substrate that is covered by veneer layers, mouldings and/or a surface coating, see Fig. 1. The substrate comprises several quarter-sawn oak boards, which are connected to form a flat structure. The veneer layers are applied plain or as marquetry, and consist of specific wood species, possibly combined with other materials, such as bone, turtle shell and ivory. The characteristics of the historical Dutch cabinet doors were systematically documented in the Rijksmuseum study [23]. This provided a useful source of information for the geometrical design of mock-ups A to F, see Fig. 3, and for the wood species, type of joints and type of veneer layers used. One practical limitation that had to be overcome related to the dimensions of the mock-up, which were restricted by the size of the climate chamber and by the limited thickness of the oak boards provided. Since this reduction in dimension was only small, the mock-up dimensions may be nevertheless considered as representative of door panels commonly present in historical cabinets.

Mock-ups A, B and D were composed of an oak substrate *restrained* by cleated ends, which does not have veneer layers attached to the front and back sides, see Fig. 3. The substrate was composed of five boards, where three boards were placed side by side with parallel grain directions. Two smaller boards, i.e., the cleated ends, were placed at the top and bottom sides of these three boards. The grain direction of the cleated ends was oriented perpendicular to the grain direction of the three boards. The three parallel boards were connected by a butt joint with animal glue, while the cleated ends were connected to the three boards by a tongue-and-grove joint with animal glue.

For mock-ups C to F the substrate was constructed in a similar fashion as described above. The effect by the cleated ends on the panel behaviour was considered by

Fig. 3 Mock-up composition. The mock-ups have a restrained (A, B, D and F) or unrestrained (C and E) oak substrate, where only mock-ups E and F have plain teak veneer layers. Animal glue is used for the joints and for the attachment of the veneer layers to the oak substrate. The grain directions in the boards and cleated ends are indicated by arrows

Luimes *et al. Herit Sci*   (2018) 6:72

Page 5 of 23

Table 1 Dimensions mock-ups

Mock-up	h	h_1	h_2	h_3	w	w_1	w_2	w_3	t
A	730.2	49.0	633.2	48.0	546.0	165.0	206.0	175.0	14.35
B	731.7	49.8	631.4	50.5	546.0	186.5	214.5	145.0	14.64
C	629.0	–	629.0	–	545.9	165.7	196.0	184.2	14.38
D	732.3	49.0	632.3	51.0	546.6	168.5	229.3	148.8	14.48
E	629.0	–	629.0	–	546.0	158.0	220.5	167.5	15.52[a]
F	732.1	48.8	634.5	48.8	545.7	160.2	216.7	168.8	15.52[a]
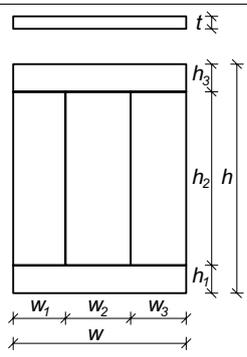
All measures are in millimetres. Note that the values not provided for h_1 and h_3 are due to the absence of cleated ends for the unrestrained mock-ups C and E

[a] The thickness of the veneer layers is equal to 0.5 mm

selecting restrained (i.e., cleated ends present) and unrestrained (i.e., cleated ends absent) oak substrates, see Fig. 3, and comparing the responses of mock-ups C and D, and mock-ups E and F. This selection was motivated from the museum study reported in [25], where for the historical door panels analysed these two types of substrates typically showed to have the most and least damage, respectively. In addition, the influence of plain teak veneer layers on the panel response was studied by considering two cases: (i) a mock-up with an unrestrained (C) or a restrained (D) substrate, but *without* veneer layers and (ii) a mock-up with an unrestrained (E) or a restrained (F) substrate *with* veneer layers at both the front and back sides. The grain directions of the veneer layers coincided with those of the three oak wooden boards below. The dimensions of mock-ups A to F are listed in Table 1.

Preparation mock-ups
The mock-ups were composed of oak boards provided by the University of Amsterdam, Faculty of Humanities, Department of Arts & Culture. The boards were stored for at least 10 years in the Ateliergebouw of the Rijksmuseum, Amsterdam at a temperature of $20\,^{\circ}C \pm 2\,^{\circ}C$ and a relative humidity of $50\% \pm 5\%$ in the winter and $55\% \pm 5\%$ in the summer. The boards were quarter-sawn, had a relatively small annual ring width between 2 and 7 mm, and almost had no imperfections, thereby accurately mimicking the high-quality characteristics of historical cabinet doors. The animal glue used for the joints and the attachment of the veneer layers to the oak substrate was composed of a solution of bone and hide glue in a ratio one to one. The water to glue ratio of the solution was two to one.

The mock-ups were made by a senior furniture conservator at the Department of Conservation and Scientific Research of the Rijksmuseum, Amsterdam. After construction, the mock-ups were kept in the Ateliergebouw of the Rijksmuseum, Amsterdam in a stable indoor climate (temperature of $20\,^{\circ}C \pm 2\,^{\circ}C$ and relative humidity of $50\% \pm 5\%$ in the winter and $55\% \pm 5\%$ in the summer). For the performance of the experimental tests, the mock-ups were transported to the climate chamber of the Structures Laboratory of the Eindhoven University of Technology, where they were kept at a temperature of $20\,^{\circ}C \pm 2\,^{\circ}C$ and a relative humidity of $60\% \pm 5\%$ for about three months. Prior to testing, the measurement devices where attached to the mock-ups, after which the mock-ups were included in the test set-up.

Test set-up
The experimental tests were performed in a Memmert ICH750 climate chamber at the Building Physics Laboratory of the Eindhoven University of Technology. The dimensions of the climate chamber are such that a homogeneous indoor climate could be ensured during testing. The mock-ups were placed in a custom-made stand in the middle of the climate chamber, whereby all surfaces were freely exposed to the surrounding air, see Fig. 4. Two layers of Teflon were placed between the mock-ups and the stand to minimize the contact friction. The wires of the measurement devices were conducted through a hole located at the backside of the climate chamber. Behind the climate chamber, the wires were connected to a data acquisition system that transmitted the measured data to a computer. The measurement time interval was set to 120 s, in order to follow the response of the mock-ups
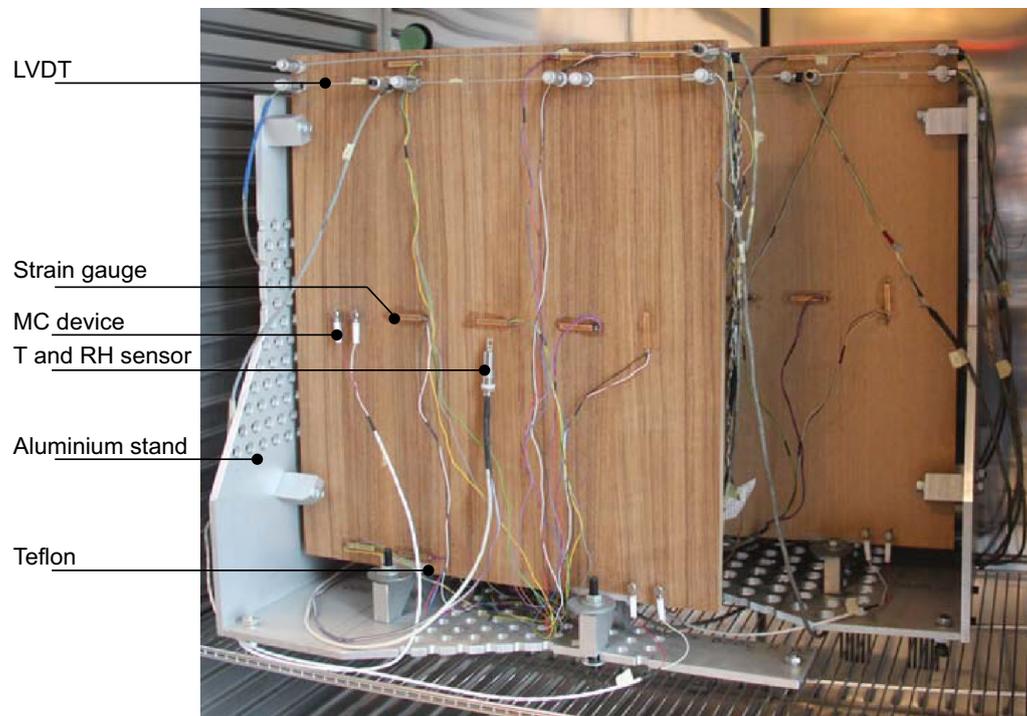
Luimes *et al. Herit Sci*   (2018) 6:72

Page 6 of 23

Fig. 4 Test set-up: mock-ups E (unrestrained substrate with veneer layers; left) and C (unrestrained substrate without veneer layers; right) inside the climate chamber
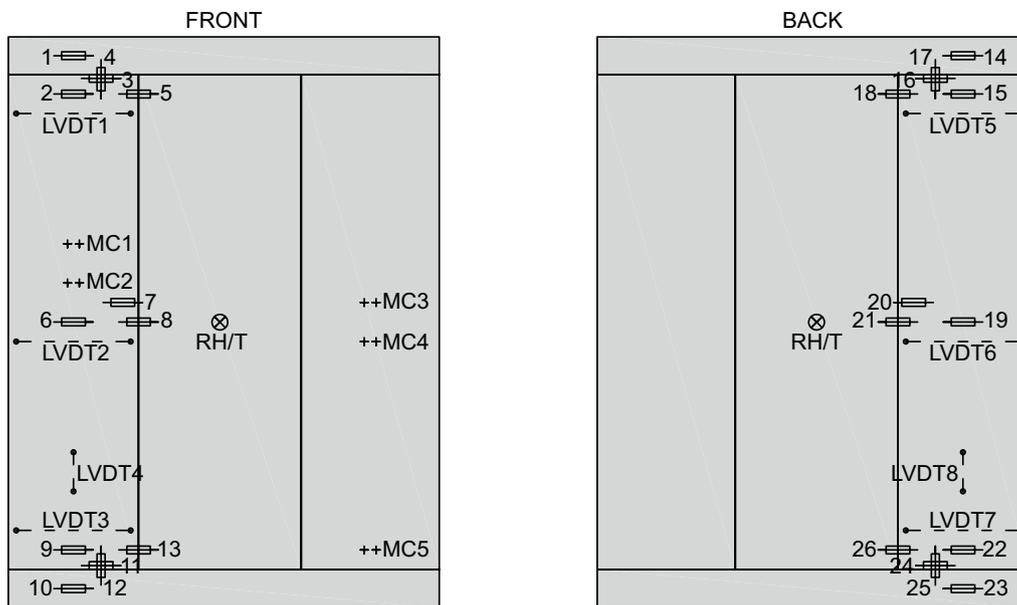
accurately while keeping the processing of the measurement data feasible.
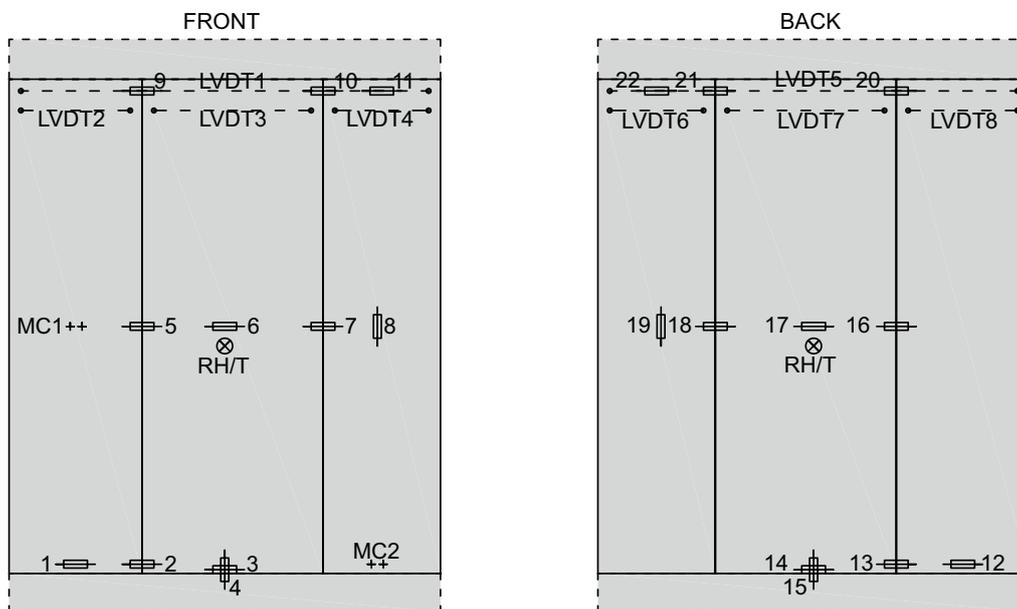
Measurements

Various measurement devices were used in order to accurately capture the hygro-mechanical response of the mock-ups. The displacement, strain, moisture content, temperature and relative humidity were monitored at a number of locations, see Fig. 5. Solartron SM3 linear variable displacement transformers (LVDTs) were glued to the mock-up surfaces to measure local displacements. A calibration was performed to check the linearity of the LVDTs, which resulted in an accuracy of ± 0.0075 mm. Tokyo Sokki Kenkyujo PFLW-30-11 strain gauges were selected to measure local strains. These special purpose strain gauges are designed for long-term measurements on wood exposed to humid conditions. A two-component hygroscopic PS polyester adhesive was used to glue the strain gauges to the mock-up surfaces. The measuring of the moisture content, which complies with EN 16682 [26], occurred at the half-depth of the mock-ups with a Brookhuis MCM Sensor (serial number 0302128), whereby the response was obtained from an indirect method based on the electrical resistance of the wood. Sorption experiments

were performed in order to calibrate the moisture content sensor. The temperature and relative humidity in the climate room were determined by using Humitter 50U/50Y(X) sensors. The sensor accuracy obtained after calibration is $\pm 0.6\,^\circ$C and $\pm 3\%$ relative humidity.

The measurement devices for mock-ups A and B were located such that the response of the left board and the response at the glue joints with the adjacent board and cleated ends were captured in detail, whereby the main purpose was to gain more insight into local dimensional changes at connections and their relation to the location of possible shrinkage cracks, see Fig. 5a. Six LVDTs were placed in horizontal direction to measure the displacement in the radial material direction of the oak wood substrate (LVDT 1, 2 and 3 on the front surface and LVDT 5, 6 and 7 on the back surface). The LVDTs were located at the middle of the board and close to the cleated ends to analyse the restraining effect of the cleated ends on the deformation response of the panel. Two vertical LVDTs were used to measure the response in longitudinal material direction of the substrate (LVDT 4 and 8 on the front and back sides, respectively). In addition, a total of 26 strain gauges was used; 13 on the front side of the mock-up and 13 on the back side. The locations of the strain gauges were selected such that the following

FRONT

1 ⊏═ 4
2 ⊏═ 3 ⊏═ 5
LVDT1

++MC1

++MC2
6 ⊏═ 7
⊏═ 8   ⊗   ++MC3
LVDT2   RH/T   ++MC4

LVDT4

LVDT3
9 ⊏═ 13
11   ++MC5
10 ⊏═ 12

BACK

17 ⊏═ 14
18 ⊏═ 16 ⊏═ 15
LVDT5

20 ⊏═
⊗ 21 ⊏═ ⊏═ 19
RH/T   LVDT6

LVDT8

LVDT7
26 ⊏═ 22
24
25 ⊏═ 23

a Mock-ups A and B.

FRONT

9 LVDT1 10 11
LVDT2   LVDT3   LVDT4

MC1++ ⊏═ 5   ⊏═ 6   ⊏═ 7 8
⊗
RH/T

1 ⊏═ ⊏═ 2   3
4   MC2
++

BACK

22 ⊏═ 21   LVDT5 20
LVDT6   LVDT7   LVDT8

19 18 ⊏═   17 ⊏═ 16 ⊏═
⊗
RH/T

14 ⊏═ 13 ⊏═ ⊏═ 12
15

b Mock-ups C to F, for which only mock-ups D and F are equipped with cleated ends.

Fig. 5 Measurement scheme for mock-ups A and B (**a**) and C to F (**b**). The locations of the displacement transformers (LVDT), strain gauges (numbers), moisture content sensors (MC) and temperature (T) and relative humidity sensors (RH) are indicated. Strain gauge group 3,11,16,24 depicted in **a** was only used on mock-up A. Strain gauge groups 3,14 and 4,15 depicted in **b** were only used on mock-ups D and F

aspects could be captured: The effect of the cleated ends on the deformation behaviour of the substrate, possible out-of-plane displacements of the substrate (warping), the orthotropic material behaviour of the oak wood substrate and the response at the glue joints. In addition,

four moisture content sensors were located at the centre of the left and right boards (MC 1 to 4), and one sensor was located at the right board, close to the cleated end (MC 5). Two temperature and relative humidity sensors (RH/T) were applied to measure the ambient climate

Luimes *et al. Herit Sci* (2018) 6:72

Page 8 of 23

conditions at the centre of the front and back surfaces of the mock-ups. Two additional temperature and relative humidity sensors were located halfway in between the mock-up surfaces and the front and back sides of the climate chamber, in order to confirm that the climate established inside the climate chamber was homogeneous; this indeed appeared to be the case.

Compared to mock-ups A and B, the locations of the measurement devices for mock-ups C to F were chosen more uniformly across the panel, such that variations of the response across the specimen could be clearly identified, see Fig. 5b. The mock-ups were equipped with eight horizontal LVDTs to measure the displacement in radial material direction (LVDT 1, 2, 3 and 4 on the front surface and LVDT 5, 6, 7 and 8 on the back surface). The LVDTs were located close to the upper cleated end, one on each of the three vertical boards and one covering the total width of the mock-ups. Mock-ups C and E were equipped with 18 strain gauges (SG 1, 2, 5–11 on the front surface and SG 12, 13, 16–22 on the back surface) and mock-ups D and F were equipped with 22 strain gauges (SG 1–11 on the front surface and SG 12–22 on the back surface). The strain gauges were positioned on the boards and across the glue joints. Two moisture content sensors (MC 1 and MC 2) were applied, one at the centre of the left board and one at the bottom of the right board. In addition, two temperature and relative humidity sensors (RH/T) were placed at the centre of the mock-ups, close to the front and back surfaces.

Time-averaged strain

From the strain profile measured the time average is determined in order to facilitate the comparison of strain responses at different measurement locations and between different mock-ups. This measure gives a good indication of how a deformation on average has evolved in time. The time average of the strain ϵ_a is characterized by the area under the strain-time curve, divided by the total time:

$$\epsilon_a = \frac{1}{t} \int_0^t \hat{\epsilon}(t)dt, \tag{1}$$

where $\epsilon = \hat{\epsilon}(t)$ is the total strain and t is the time.

Boundary conditions

The relative humidity profiles applied to the mock-ups are depicted in Fig. 6. Mock-ups A and B were subjected to single and multiple *stepwise decreasing* relative humidity profiles, respectively, as depicted in Fig. 6a and b. The temperature was kept constant at 20 °C. For both profiles the total drop in relative humidity is from 60 to 20%, with the total duration of the humidity profiles being

comparable. These humidity changes obviously are larger than those currently defined as acceptable for indoor museum conditions; nonetheless, they are assumed to be representative of the more extreme, uncontrolled variations experienced during manufacturing and the early history of the museum object. Mock-ups C to F were subjected to a *continuously varying* relative humidity profile (at a constant temperature of 20 °C) illustrated in Fig. 6c. This humidity profile is based on measurement data obtained from the Grand Salon of the Amerongen Castle, located in Amerongen, The Netherlands. The measurement data were provided by the Chair of Building Physics of the Eindhoven University of Technology, and were obtained by measuring the indoor climate in the Grand Salon from 2010 until 2014 [12]. During this 4-year period, the largest fluctuations in relative humidity were measured in the winter of 2012, from 26 January to 24 February, which were used as a basis for the humidity profile applied in the experiments. Note from Fig. 6c that the experimental relative humidity profile varies between 35 and 71%, and slightly differs from the measured profile in the Amerongen Castle; however, since the differences are small, the experimental profile may be assumed to be representative of the measured climate conditions. Considering that cabinet door panels in museums typically are exposed to climate conditions that are much more strict, this humidity profile can be regarded as a serious test case for the damage resistance of door panels.

Experimental results mock-ups A and B
### Deformation response

The time evolutions of horizontal strains measured in mock-ups A and B are, respectively, depicted in Figs. 7 and 8 for a selection of strain gauges. In accordance with Fig. 5a, the strain gauges selected can be assembled in groups with a similar location, which is the group of strain gauges 6,19 attached to one of the three boards at the half-length of the panel, the group 2,9,15,22 attached to one of the boards near a cleated end, and the group 1,10,14,23 attached to a cleated end. The strain responses of the first two groups are depicted in Figs. 7a and 8a, while the response of the latter group is shown in Figs. 7b and 8b, together with the corresponding relative humidity profile taken from Fig. 6. The responses measured by the other strain gauge groups shown in the overview of Fig. 5a are omitted in Figs. 7 and 8, since the trends are qualitatively similar to those of the three strain gauge groups depicted. For completeness, however, further in this communication the time-averaged strain value and the final strain value measured by these additional strain gauge groups will be analysed and compared to the time-averaged values of the current three strain gauge groups.

Luimes *et al. Herit Sci* (2018) 6:72

Page 9 of 23
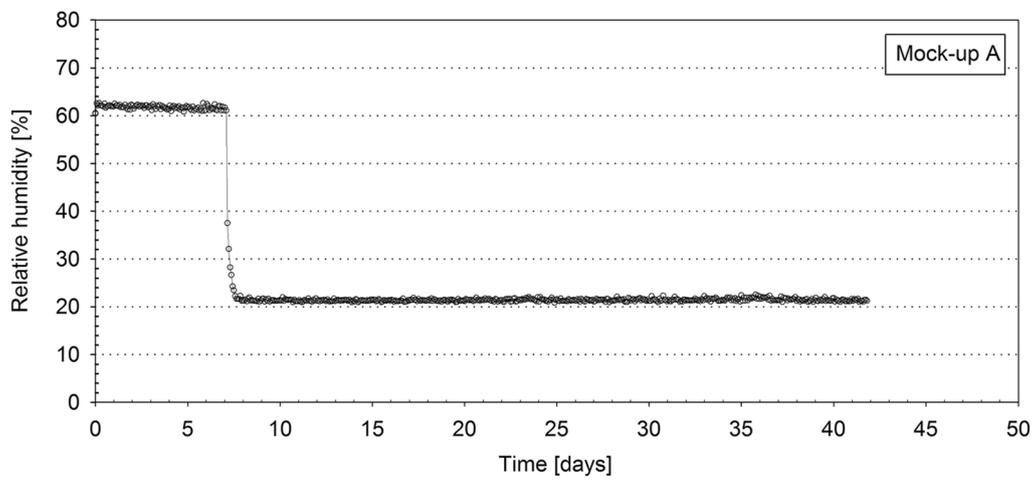
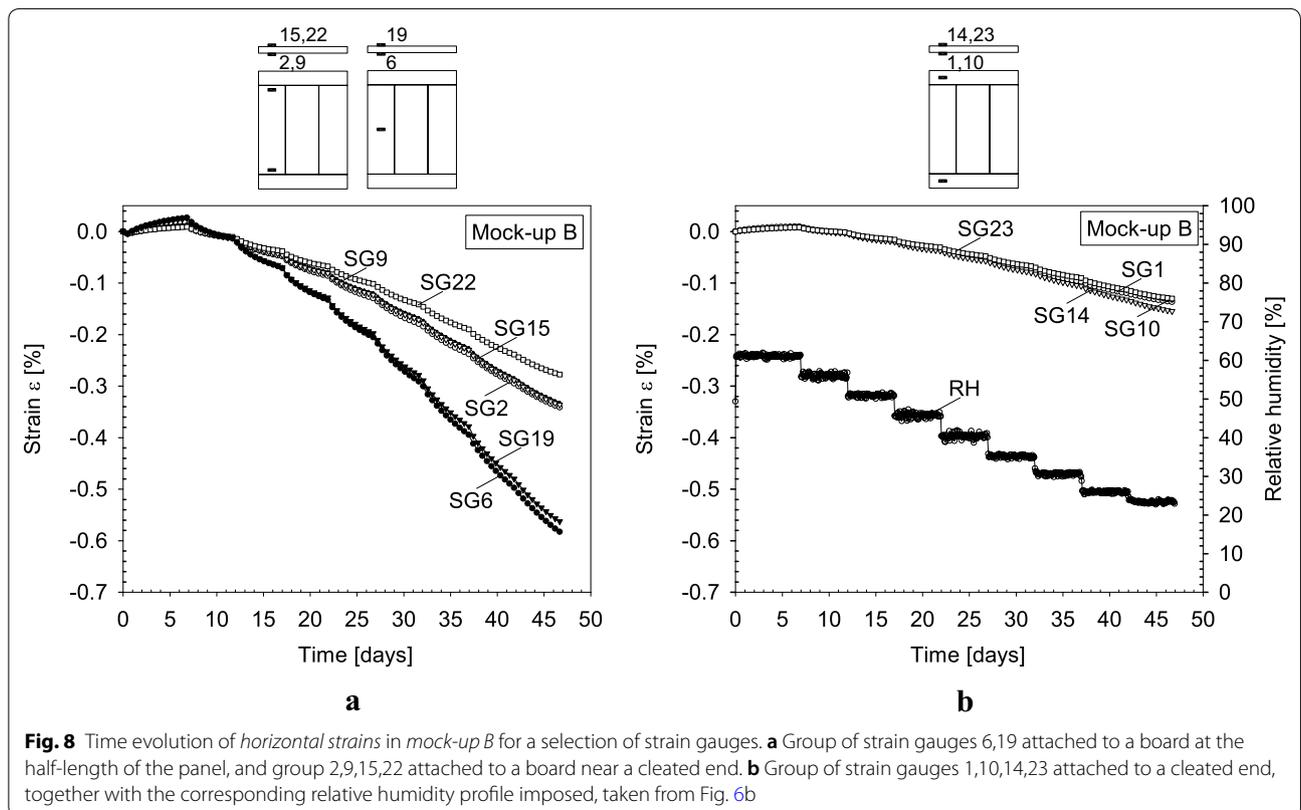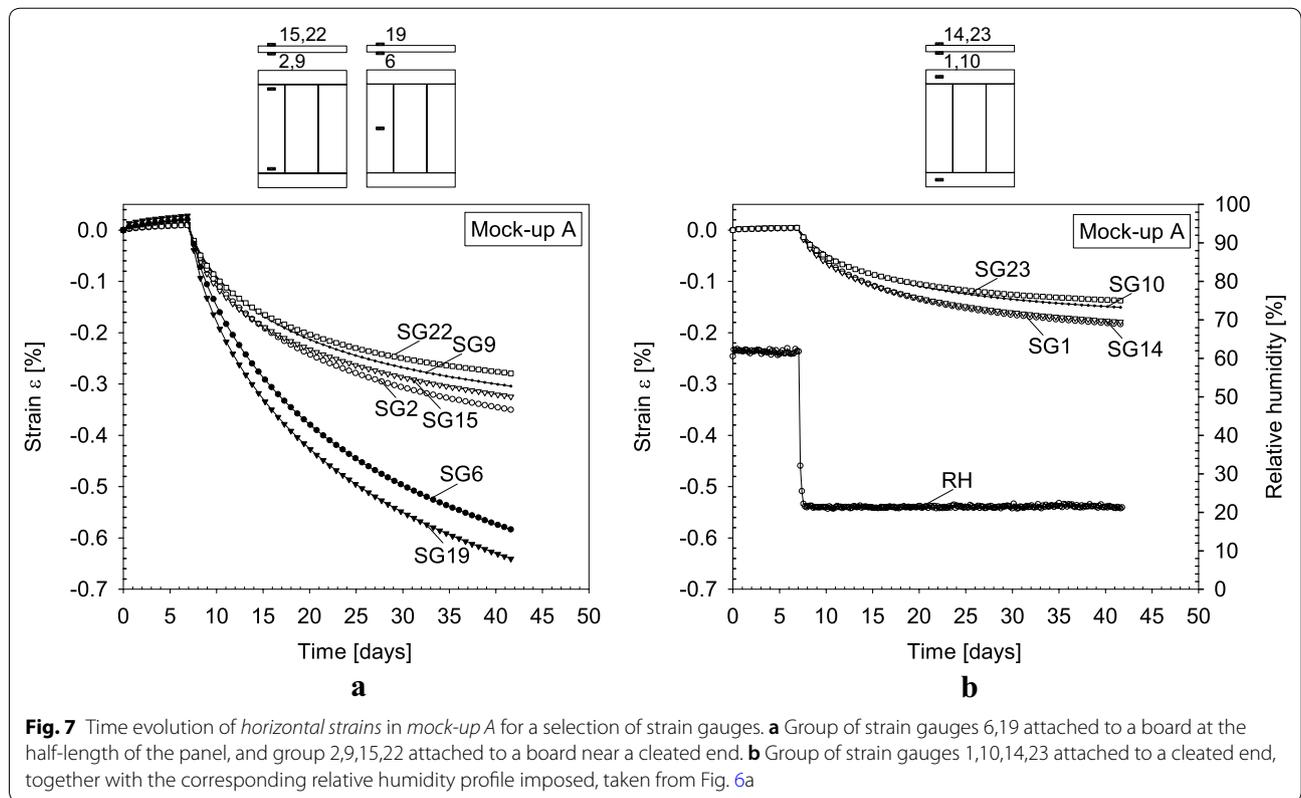**a** Time evolution of the relative humidity for mock-up A.
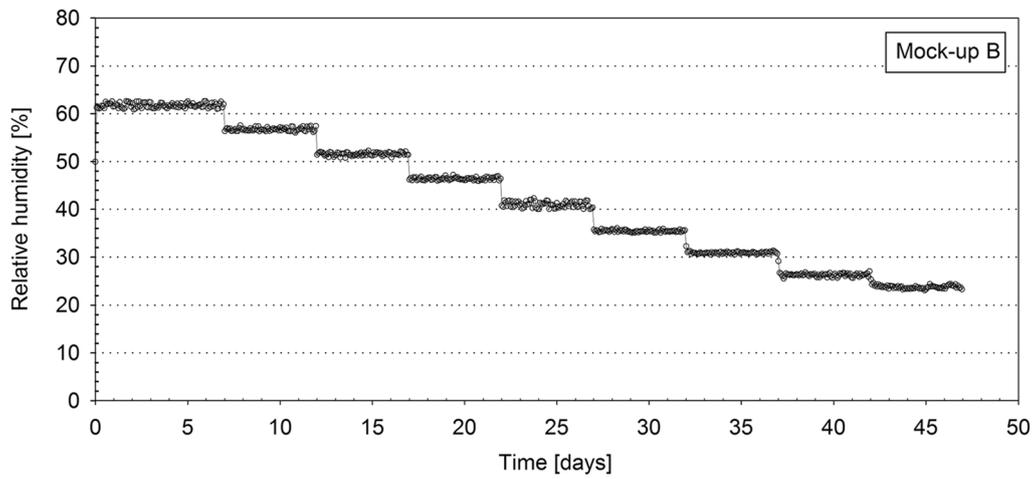
b Time evolution of the relative humidity for mock-up B.
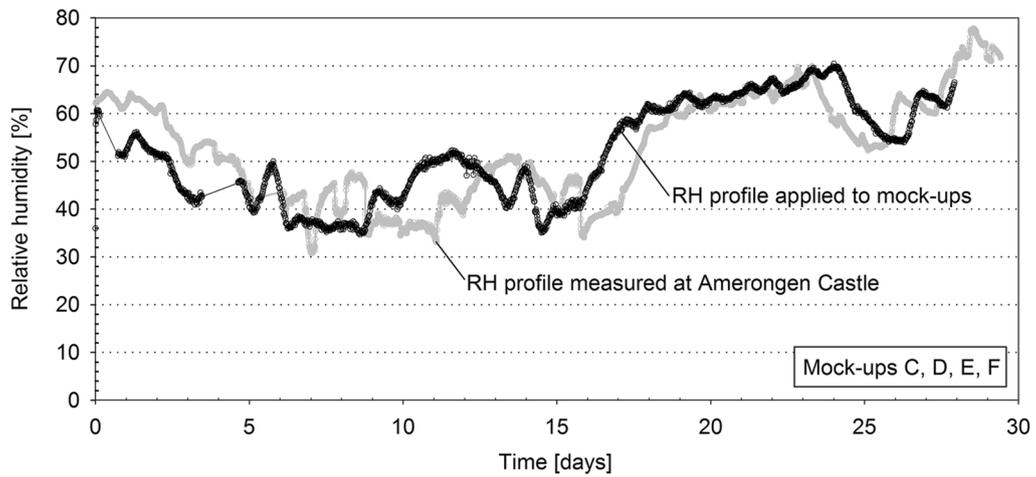
c Time evolution of the relative humidity for mock-ups C to F.

Fig. 6 Time evolution of the relative humidity applied to mock-ups A (**a**), B (**b**) and C to F (**c**). During testing the temperature was kept constant at 20 °C

Fig. 7 Time evolution of *horizontal strains* in *mock-up A* for a selection of strain gauges. **a** Group of strain gauges 6,19 attached to a board at the half-length of the panel, and group 2,9,15,22 attached to a board near a cleated end. **b** Group of strain gauges 1,10,14,23 attached to a cleated end, together with the corresponding relative humidity profile imposed, taken from Fig. 6a

Fig. 8 Time evolution of *horizontal strains* in *mock-up B* for a selection of strain gauges. **a** Group of strain gauges 6,19 attached to a board at the half-length of the panel, and group 2,9,15,22 attached to a board near a cleated end. **b** Group of strain gauges 1,10,14,23 attached to a cleated end, together with the corresponding relative humidity profile imposed, taken from Fig. 6b

During the first 7 days the relative humidity was kept fixed at 60%, whereby the strain profiles shown in Figs. 7 and 8 for mock-ups A and B remained approximately constant. After 7 days the relative humidity was lowered to 20% in a single step for mock-up A, and in eight separate steps of 5% for mock-up B. It can be observed that the *slopes* of the strain profiles measured for mock-up A initially are high, but gradually decrease to relatively small values observed at the end of the hygral loading process, indicating that the final response of mock-up A is close to the time-independent steady-state limit. Mock-up B experiences incremental changes in deformation each time the relative humidity is lowered by 5%, which causes the overall trend of the strain curves to be different from that for mock-up A. The final strain values of the two mock-ups are comparable, and are the largest for strain gauge group 6,19 attached to one of the three boards at the half-length of the panel, followed by strain gauge group 2,9,15,22 attached to one of the boards near a cleated end, and finally the group 1,10,14,23 attached to a cleated end. This clearly indicates that the restraining effect by the cleated end on the local deformation response of the substrate decreases with increasing distance from the cleated end. The relatively small horizontal deformations measured *on* the cleated ends are mainly due to the coefficient of hygroscopic expansion in the

longitudinal material direction of the oak wooden cleated ends being more than 10 times smaller than that in the radial material direction of the oak wooden boards [27]. Note finally that the strain measurements within a strain gauge group show some spread in value, which may be mainly ascribed to the spatial heterogeneity of the oak wood microstructure.

The time evolutions of the local panel displacements measured by the LVDTs are depicted in Fig. 9a and b for mock-ups A and B, respectively. From a comparison with Figs. 7 and 8, it can be confirmed that the horizontal displacements (recorded by LVDT 2, 6) follow a similar trend as that recorded by the horizontal strain gauges. The final displacements measured across an individual oak wooden board (as obtained by LVDT 2, 6) are comparable to those following from multiplying the local values measured by strain gauges at similar locations (i.e., SG 6, 19) with the corresponding nominal LVDT width. The relative differences between these global and local deformation measures for the two mock-ups fall in between 3 and 35%, and indicate that the deformation across a board is not ideally uniform, due to the heterogeneity of the oak wood microstructure. It is further noted that for mock-up B the horizontal displacements measured at the back side of the panel (LVDT 5, 6 and 7) are up to 34% lower compared to the corresponding
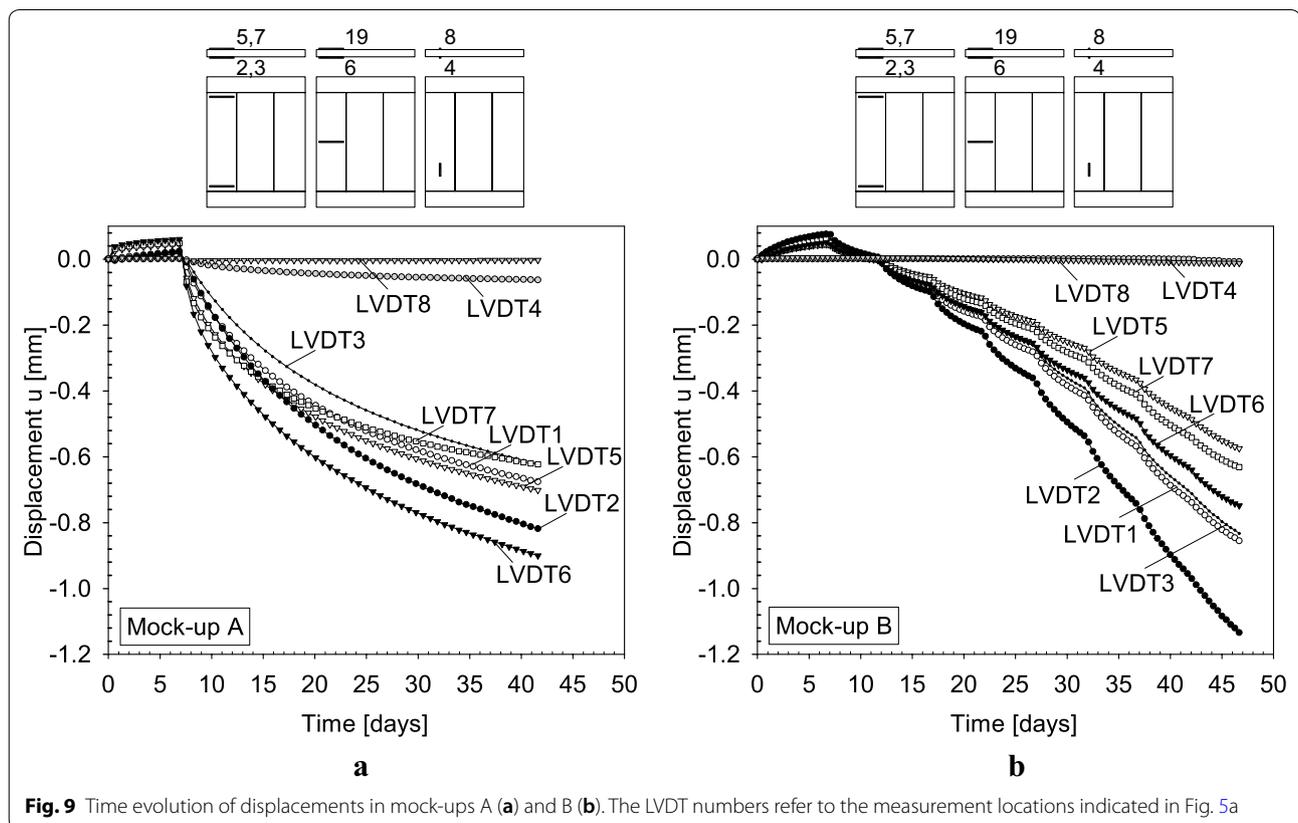

Fig. 9 Time evolution of displacements in mock-ups A (**a**) and B (**b**). The LVDT numbers refer to the measurement locations indicated in Fig. 5a

Luimes *et al. Herit Sci*   (2018) 6:72

Page 12 of 23

displacements at the front side of the panel (LVDT 1, 2 and 3), see Fig. 9b. This difference may be ascribed to the fact that the left board of mock-up B is not ideally quarter-sawn, as a result of which the material orientation rotates counter clockwise going from the right side to the left side of the board, see Fig. 10. Consequently, the board is subjected to some warping, induced by a lower shrinkage at the back side than at the front side. Finally, it shows that the *vertical* displacements of the oak wooden board measured by LVDT 4 and 8 are negligible, which results from the fact that the coefficient of hygroscopic expansion in the longitudinal material direction of the oak wooden board (= vertical panel direction) is more than 10 times smaller than in its radial material direction (= horizontal panel direction).

The time-averages of all strain measurements shown in the overview in Fig. 5a are calculated in accordance with Eq. (1), and depicted in Fig. 11 by means of the average
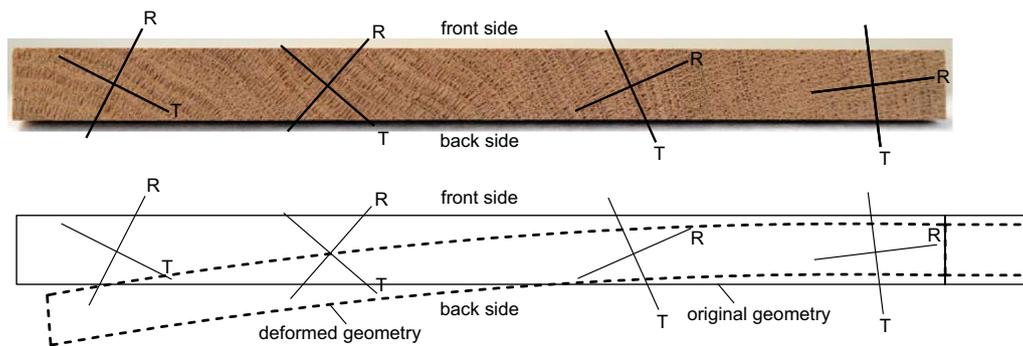

Fig. 10 Spatial variation in the orientation of R–T material axes in the not perfectly quarter-sawn left board of mock-up B, together with a schematic representation of the resulting warping under a drop in relative humidity. The warped shape of the board has been validated by means of a finite element simulation not presented here for brevity
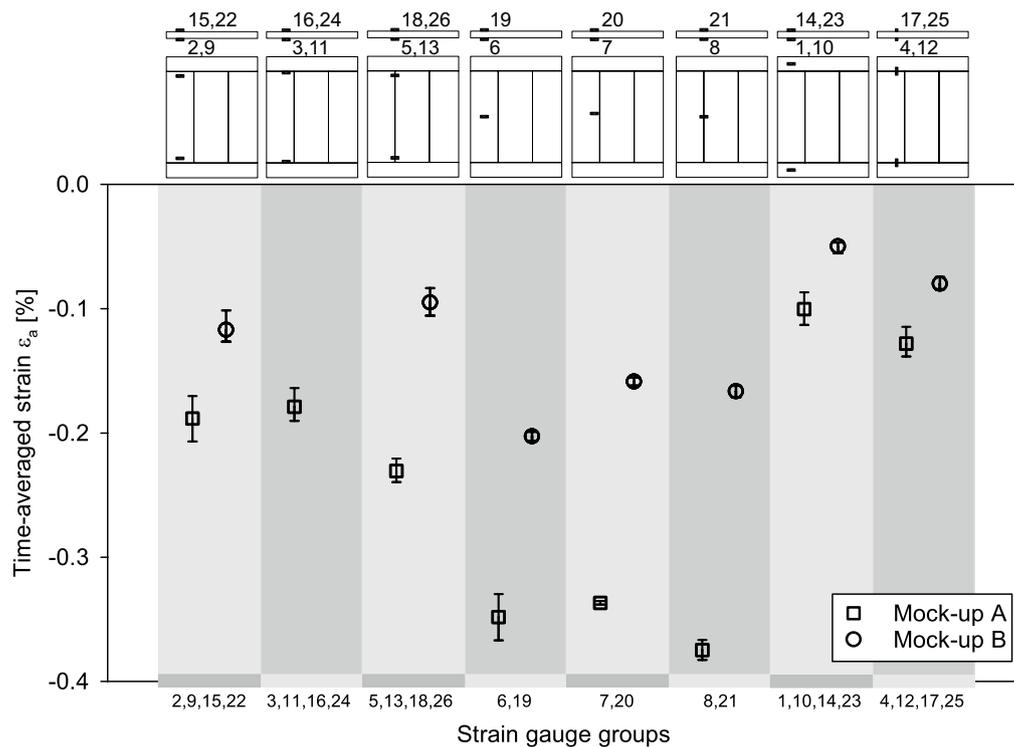

Fig. 11 Overview of the *time-averaged* strain per strain gauge group. The numbers along the horizontal axis define the strain gauge groups and correspond to the measurement locations indicated in Fig. 5a. The squares and circles indicate the mean values for mock-ups A and B, respectively. The bars indicate the minimal and maximal time-averaged strains recorded at specific locations within a strain gauge group. Note that strain gauge group 3,11,16,24 was only used on mock-up A

per strain gauge group. As already explained, a strain gauge group is composed of strain gauges positioned at similar measurement locations. It can be observed that the time-averaged strains recorded for mock-up A are always substantially larger than those for mock-up B, see Fig. 11. This clearly results from the less abrupt decrease in relative humidity for mock-up B, whereby the deformation generated develops in a more gradual fashion, see also Figs. 7 and 8, leading to a lower value for the time-averaged strain ϵ_a. Note that all time-averaged strain values are negative, generally reflecting a *shrinkage behaviour* of the panel. The strain values observed at the half-length of the panel, i.e., the values measured by strain gauge groups 6,19, 7,20 and 8,21 are similar, which illustrates that it is insignificant whether the strain gauge is located on a single board, or on two adjacent boards thereby crossing a glue connection. Accordingly, it may be concluded that the glue does not fail, and that the elastic stiffness of the glue connection is much larger than of the oak wood itself (so that it does not influence the deformation behaviour of the panel). The same conclusion may be drawn after comparing the horizontal strains of the strain gauge groups 2,9,15,22, 3,11,16,24 and

5,13,18,26 located on boards near a cleated end. Also, the vertical strain gauges across the glue joint between the cleated end and the boards, i.e., strain gauge group 4,12,17,25, did not give an indication of failure of the glue connection; the strain values measured by this strain gauge group almost completely result from the deformation of the cleated end in the radial material direction.

In addition to the computation of the mean value of the *time-averaged* strains over a strain gauge group, the mean value of the *final* strain (i.e., the strain value at the end of the hygral loading process) has been derived from the strain measurements, see Fig. 12. The final shrinkage strain obviously has a larger value than the time-averaged shrinkage strain plotted in Fig. 11. Further, moderate to small differences appear in the values recorded for mock-ups A and B; this indicates that the final deformations of the mock-up only slightly depend on how the overall drop in 40% relative humidity is applied in time. The largest value of the final shrinkage strain occurs at the half-length of the panel, i.e., at the strain gauge groups 6,19, 7,20 and 8,21, at which location the restraining effect by the cleated end is expected to be negligible (which will be confirmed in
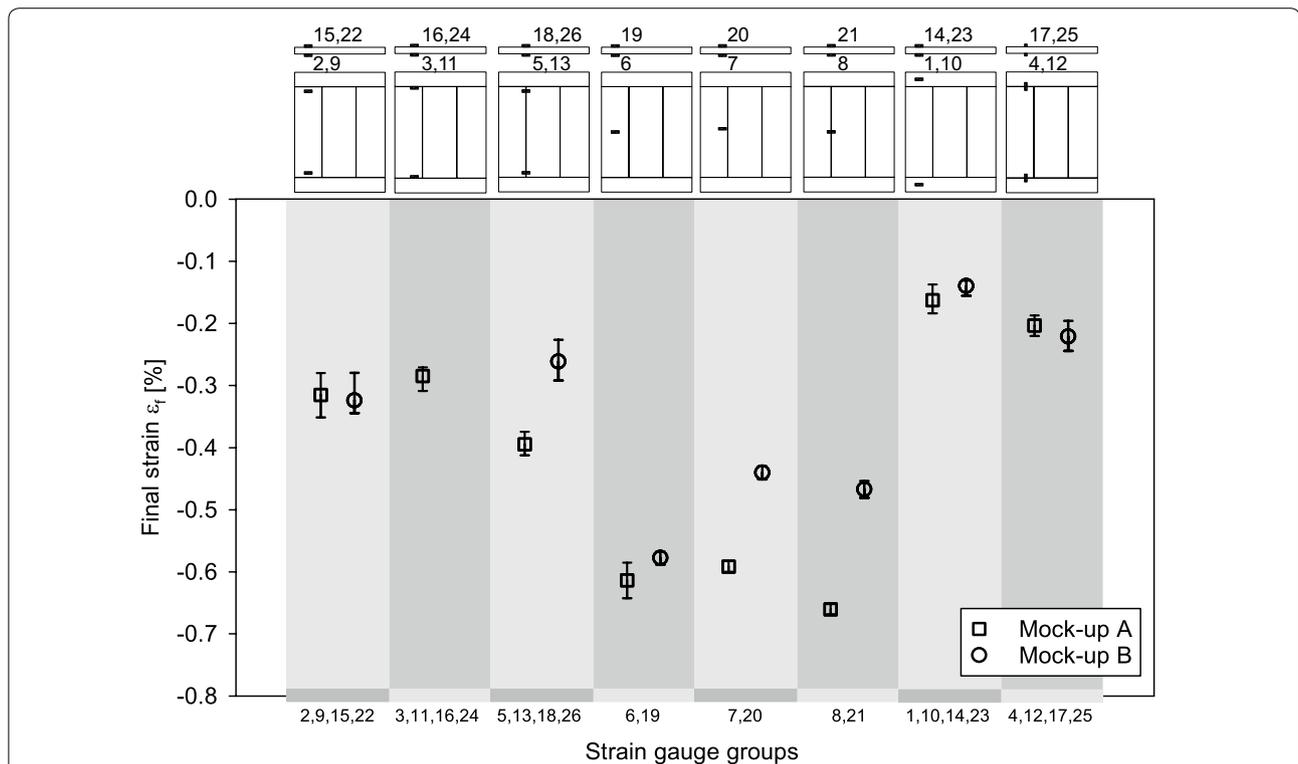

Fig. 12 Overview of the *final* strain per strain gauge group. The numbers along the horizontal axis define the strain gauge groups and correspond to the measurement locations indicated in Fig. 5a. The squares and circles indicate the mean values for mock-ups A and B, respectively. The bars indicate the minimal and maximal final strains recorded at specific locations within a strain gauge group. Note that strain gauge group 3,11,16,24 was only used on mock-up A

Luimes *et al. Herit Sci* (2018) 6:72

Page 14 of 23

the "Experimental results mock-ups C, D, E and F" section). The values measured by these strain gauge groups lie between -0.43 and -0.67%, which, in accordance with a panel width of 546 mm, relates to a horizontal shortage of the panel between 2.3 and 3.7 mm. Near the cleated ends, i.e., at the strain gauge groups 2,9,15,22, 3,11,16,24 and 5,13,18,26, the final shrinkage strains in the substrate are almost a factor of two lower, in between -0.23 and -0.41%. The final shrinkage strain measured *on* the cleated ends, i.e., at the strain gauge group 1,10,14,23, is the lowest, and varies between -0.13 and -0.18%, which is mainly due to the relatively small hygroscopic expansion coefficient in the longitudinal material direction of the cleated end. A more detailed interpretation of the local shrinkage strains and their relation to the occurrence of damage in the panel is provided in the next section.

Restrained shrinkage and risk of damage

The spatial variety in the shrinkage strains measured across the panel may have different origins. Consider, for example, the strain responses plotted in Fig. 7a and b for strain gauges SG6 and SG10 attached to mock-up A and oriented in the radial and longitudinal material directions of the oak wood, respectively (see Fig. 5a), or the displacement responses illustrated in Fig. 9a, measured by LVDT 3 and 4 in the radial and longitudinal material directions, respectively. The reason that the deformation in the radial material direction here is larger than in the longitudinal material direction can be mainly ascribed to the considerable difference of a factor of 10 in the corresponding hygroscopic expansion coefficients of orthotropic oak wood [27]. Other aspects that can be seen as a cause for the difference in the amount of shrinkage observed on the panel surfaces are the mock-up composition, the local wood density (a large annual ring width results in more shrinkage than a small annual ring width), a variation in moisture content across the thickness of the panel, and the appearance of spatial changes in the orthotropic material directions (e.g., not perfectly quarter-sawn boards and the presence of conical or spiral grain directions).

In order to explore how local differences in shrinkage behaviour may influence the susceptibility of the panel to damage, it is useful to consider the in-plane response of the hygro-elastic bi-layer illustrated in Fig. 13. The two layers constructing the bi-layer are orthotropic, initially stress-free, and are connected by a coherent ($=$ fully sticking) interface. The in-plane hygro-mechanical behaviour of the orthotropic bi-layer is characterized by the elasticity parameters $E_x^{(i)}$, $E_z^{(i)}$ and $\nu_{zx}^{(i)}$, the hygroscopic expansion coefficients $\beta_x^{(i)}$ and $\beta_z^{(i)}$, and the layer heights $h^{(i)}$, with the indices $i = 1, 2$ designating the individual layers. Driven by a change in moisture content $\Delta m^{(i)}$ (defined as the mass of moisture per unit volume divided by the mass of dry material per unit volume), layer-wise uniform stresses are generated. The normal stresses $\sigma_{xx}^{(i)}$ can be computed by starting from static equilibrium of the bi-layer in x-direction:

$$\sigma_{xx}^{(1)} h^{(1)} + \sigma_{xx}^{(2)} h^{(2)} = 0. \tag{2}$$

In addition, the total axial strain $\epsilon_{xx}^{(i)}$ experienced by each layer may be decomposed into an elastic part $\epsilon_{xx}^{e,(i)}$ and a hygroscopic part $\epsilon_{xx}^{m,(i)}$:

$$\epsilon_{xx}^{(i)} = \epsilon_{xx}^{e,(i)} + \epsilon_{xx}^{m,(i)} \qquad \text{with} \qquad i = 1, 2, \tag{3}$$

where the superindex m used for the hygroscopic strain refers to "moisture". Under *plane-stress* conditions (i.e., $\sigma_{zz} = 0$), the elastic and hygroscopic strains in each layer can be derived from the general constitutive expressions for an orthotropic hygro-elastic continuum as

$$\epsilon_{xx}^{e,(i)} = \frac{\sigma_{xx}^{(i)}}{E_x^{(i)}} \qquad \text{and} \qquad \epsilon_{xx}^{m,(i)} = \beta_x^{(i)} \Delta m^{(i)}, \tag{4}$$

while under *plane-strain* conditions (i.e., $\epsilon_{zz} = 0$) these two strains follow as

$$\epsilon_{xx}^{e,(i)} = \frac{\sigma_{xx}^{(i)}}{E_x^{(i)}} \left(1 - (\nu_{zx}^{(i)})^2 \frac{E_x^{(i)}}{E_z^{(i)}} \right) + \nu_{zx}^{(i)} \beta_z^{(i)} \Delta m^{(i)} \quad \text{and}$$

$$\epsilon_{xx}^{m,(i)} = \beta_x^{(i)} \Delta m^{(i)}. \tag{5}$$

The first expression in Eq. (5) has been obtained by making use of the symmetry condition $\nu_{xz} E_z = \nu_{zx} E_x$ of the orthotropic elastic tensor. Inserting either Eq. (5) or Eq. (4) for each of the two layers into Eq. (3), followed by
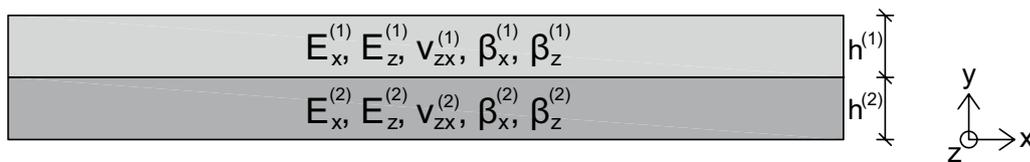

Fig. 13 Orthotropic hygro-elastic bi-layer composed of layers (1) and (2)

equating the two resulting expressions and invoking Eq. (2), allows for computing the stresses $\sigma_{xx}^{(i)}$ in each layer as

$$\sigma_{xx}^{(1)} = \frac{(\bar{\beta}_x^{(2)} \Delta m^{(2)} - \bar{\beta}_x^{(1)} \Delta m^{(1)}) h^{(2)} \bar{E}_x^{(1)} \bar{E}_x^{(2)}}{h^{(1)} \bar{E}_x^{(1)} + h^{(2)} \bar{E}_x^{(2)}},$$

$$\sigma_{xx}^{(2)} = -\sigma_{xx}^{(1)} \frac{h^{(1)}}{h^{(2)}}, \tag{6}$$

where under *plane-stress* conditions the *effective* stiffness $\bar{E}_x^{(i)}$ and the *effective* hygroscopic expansion coefficient $\bar{\beta}_x^{(i)}$ of a layer are given by

$$\bar{E}_x^{(i)} = E_x^{(i)} \qquad \text{and} \qquad \bar{\beta}_x^{(i)} = \beta_x^{(i)}, \tag{7}$$

while under *plane-strain* conditions these parameters are

$$\bar{E}_x^{(i)} = \frac{E_x^{(i)}}{1 - \left(\nu_{zx}^{(i)}\right)^2 \frac{E_x^{(i)}}{E_z^{(i)}}} \qquad \text{and}$$

$$\bar{\beta}_x^{(i)} = \left(1 + \nu_{zx}^{(i)} \frac{\beta_z^{(i)}}{\beta_x^{(i)}}\right) \beta_x^{(i)}. \tag{8}$$

Equation (6) shows that the two layers develop stresses under the following two basic types of conditions: *Type 1*, where the change in moisture content in each layer is different, $\Delta m^{(1)} \neq \Delta m^{(2)}$, but their effective coefficients of hygroscopic expansion are equal, $\bar{\beta}_x^{(1)} = \bar{\beta}_x^{(2)}$, and *Type 2*, where the change in moisture content in both layers is equal, $\Delta m^{(1)} = \Delta m^{(2)}$, but the effective hygroscopic expansion coefficients are different, $\bar{\beta}_x^{(1)} \neq \bar{\beta}_x^{(2)}$. Trivially, combinations of these two basic cases, i.e., mutual differences in *both* the moisture content and the effective coefficient of hygroscopic expansion, will also lead to stresses in the layers, in accordance with the general condition $\bar{\beta}_x^{(1)} \Delta m^{(1)} \neq \bar{\beta}_x^{(2)} \Delta m^{(2)}$. It can be further observed from Eq. (6) that the stresses in the two layers have an opposite sign, i.e., if one layer is subjected to compression (characterized by a negative sign of the stress), the other layer is subjected to tension (characterized by a positive sign of the stress).

The result given by Eq. (6) can be used for identifying the origin of locally restrained hygral shrinkage in the panel, and its effect upon crack formation. For mock-ups A and B, restrained hygral shrinkage may originate from: (i) a difference in moisture content across the thickness direction of the boards, i.e., *Type 1* shrinkage, or (ii) a directional difference in the coefficients of hygroscopic expansion of structural components forming a coherent connection, i.e., *Type 2* shrinkage. Type 1 shrinkage occurs in the outer regions of the board thickness; these

regions initially experience a relatively fast decrease in moisture content upon a decreasing relative humidity at the front and back sides of the board, while the inner core of the board has not (yet) experienced a noticeable change in moisture concentration. When considering one of these outer regions as layer 1 and half of the core of the boards as layer 2 (thereby making use of the symmetry across the thickness direction), in accordance with Eq. (6) this results into a tensile stress in the outer regions of the board thickness and a compressive stress at the core, see also the qualitative sketch in Fig. 14. Conversely, Type 2 shrinkage occurs at the cleated ends of a panel, where the longitudinal (grain) direction of the oak wood representing the cleated end is oriented perpendicular to that of the connecting boards composing the substrate. The coefficient of hygroscopic expansion in the radial material direction of the boards is larger than in the longitudinal material direction of the cleated end. When interpreting the cleated end as layer 1 and the upper region of the boards adjacent to the cleated end as layer 2, in accordance with Eq. (6) the boards will be subjected to tension and the cleated end will be loaded in compression, see also the qualitative sketch in Fig. 15.
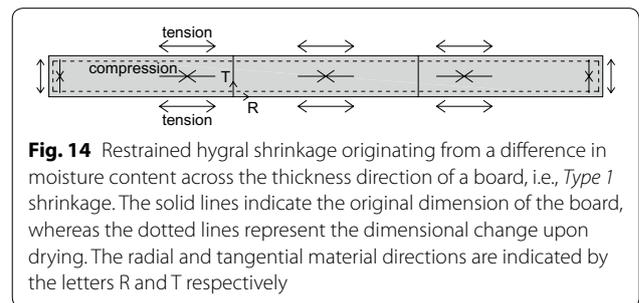

Fig. 14 Restrained hygral shrinkage originating from a difference in moisture content across the thickness direction of a board, i.e., *Type 1* shrinkage. The solid lines indicate the original dimension of the board, whereas the dotted lines represent the dimensional change upon drying. The radial and tangential material directions are indicated by the letters R and T respectively
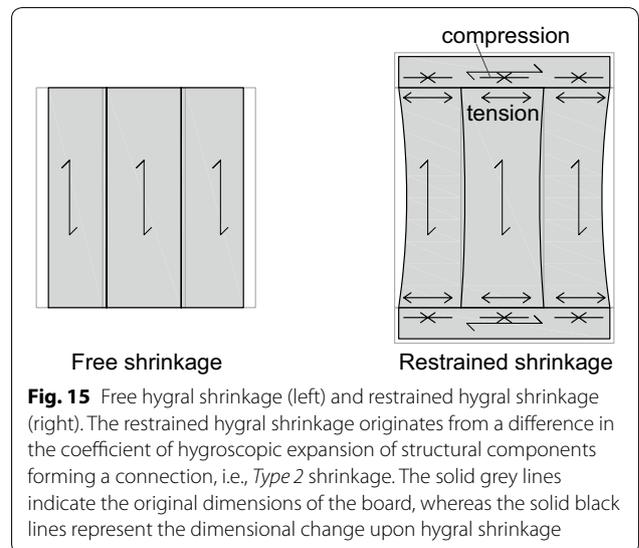

Fig. 15 Free hygral shrinkage (left) and restrained hygral shrinkage (right). The restrained hygral shrinkage originates from a difference in the coefficient of hygroscopic expansion of structural components forming a connection, i.e., *Type 2* shrinkage. The solid grey lines indicate the original dimensions of the board, whereas the solid black lines represent the dimensional change upon hygral shrinkage

Luimes *et al. Herit Sci*   (2018) 6:72

Page 16 of 23

Table 2 Elasticity parameters (taken from [28]) and hygroscopic expansion coefficients (taken from [27]) in the longitudinal (L) and radial (R) material directions of oak wood

Elasticity parameters	E_L [N/mm^2]	12,800
	E_R [N/mm^2]	1600
	ν_{LR} [–]	0.35
Hygroscopic expansion coefficients	β_L [-]	0.016
	β_R [–]	0.19

Correspondingly, the glued tongue-and-grove joints between the boards and cleated ends will be loaded in shear and the glued butt joints between the boards will be loaded in tension.

In order to compute the tensile stresses in the mock-ups for both types of restrained hygral shrinkage, the material parameters for oak wood as listed in Table 2 are used. Here, the elastic moduli are adopted from [28] and the hygroscopic expansion coefficients are taken from [27]. Starting with the analysis of Type 1 shrinkage across the thickness of the oak wooden boards, it is assumed that the oak wood at the half-length of the boards is subjected to *plane-strain* conditions in the length (= vertical) direction of the panel, in correspondence with the negligible deformations measured by LVDT 4 and 8 in the length direction of mock-ups A and B, see Fig. 9. The *x*- and *z*-directions of the bi-layer thus correspond to the radial and longitudinal material directions of the oak wooden boards, respectively. Consider now a drop in relative humidity from 60 to 20%, which relates to a *maximal* drop in moisture content in the oak wood from 0.089 to 0.051, in accordance with the values at points A and B in Fig. 16 (these values will be further discussed in the "Moisture content development" section). Under the assumption that the maximal drop in moisture content takes place in the outer quarter regions across the board thickness h, i.e., $\Delta m^{(1)} = 0.059 - 0.089 = -0.038$ for $h^{(1)} = h/4$, and the moisture content of the inner core of the boards does not change, i.e., $\Delta m^{(2)} = 0$ for $h^{(2)} = h/4$ (representing half of the symmetrical inner core), Eq. (6) provides a tensile stress in the outer quarter region of $\sigma_{xx}^{(1)} = 6.0$ N/mm^2. This tensile stress lies below the values for the tensile strength (measured perpendicular to the grain direction) of new oak wood (≈ 21 N/mm^2) and seventeenth century oak wood (≈ 12 N/mm^2) reported in [28]. Note hereby that the latter strength value is substantially lower, which is the result of aging effects. From these strength data it may be concluded that under the current Type 1 shrinkage conditions cracking indeed does not occur, also not if the panel tested would have been made of (weaker) seventeenth century oak wood. The horizontal shrinkage strain under the above Type 1
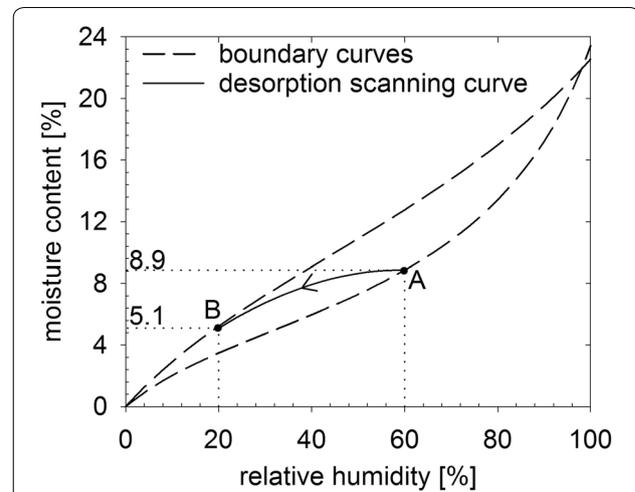

Fig. 16 Moisture hysteresis behaviour of oak wood. The boundary curves reflecting time-independent (steady-state) hygral equilibrium are indicated by dashed lines, and were determined by means of sorption tests. The desorption scanning curve indicated by a solid line is constructed with the hysteresis model presented in [29]

conditions can be computed from Eqs. (3) and (5), and for both layers equals $\epsilon_{xx} = -0.37\%$. Obviously, this shrinkage strain lies below the range of final horizontal shrinkage strains of -0.6% to -0.7% that was measured for mock-up A at strain gauge groups 6,19, 7,20 and 8,21, see Fig. 12. The reason for this is that the measured final shrinkage strain is expected to agree closely to the steady-state situation, whereby the board has undergone sufficient time to accommodate for the maximal drop in moisture content across its *complete thickness*, i.e., $\Delta m^{(1)} = \Delta m^{(2)} = -0.038$. Indeed, with a uniform coefficient of hygroscopic expansion across the board thickness, Eq. (6) confirms that the stresses relax to zero, $\sigma_{xx}^{(1)} = \sigma_{xx}^{(2)} = 0$, which, with Eqs. (3) and (5), leads to a maximal final horizontal shrinkage strain of the layers of $\epsilon_{xx} = -0.74\% (= \bar{\beta}_x \Delta m = \bar{\beta}_x(m_B - m_A))$. This value for the final shrinkage strain is only slightly larger than the measured values plotted in Fig. 12.

For a Type 2 shrinkage analysis at the cleated ends, a *plane-stress* assumption is taken, in agreement with the limited thickness of the cleated ends and the boards in the out-of-plane direction. Hence, in the bi-layer model the stress response only depends on the material characteristics in the *x*-direction, see Eqs. (6) and (7). The elastic moduli and the hygroscopic expansion coefficients are again taken from Table 2, whereby the *x*-direction of the bi-layer is represented by the longitudinal direction of the oak wooden cleated end (= layer (1)), and by the radial direction of the oak wooden boards (= layer (2)). The effective height $h^{(2)}$ across which the oak wooden board substantially contributes to the local hygral-mechanical

Luimes *et al. Herit Sci* (2018) 6:72

Page 17 of 23

equilibrium near the cleated end is assumed to be equal to the height $h^{(1)}$ of the cleated end. Under a maximal drop in moisture content of $\Delta m^{(1)} = \Delta m^{(2)} = -0.038$, Eq. (6) provides a tensile stress in the oak wooden board of $\sigma_{xx}^{(2)} = 9.4\,\text{N/mm}^2$. With this result, the total horizontal shrinkage strain in the layers from Eq. (3) is calculated as $\epsilon_{xx} = -0.13\%$, which is indeed comparable to the total final shrinkage strain measured for mockup A on the cleated end, see Fig. 12 for the strain gauge group 1,10,14,23. This agreement confirms that the above assumption for the effective height $h^{(2)}$ of the oak wooden board is realistic. Note that the above tensile stress does not exceed the tensile strength of new oak wood of $21\,\text{N/mm}^2$ (measured perpendicular to the grain direction), as reported in [28]; however, the stress has a magnitude relatively close to the reported tensile strength of $12\,\text{N/mm}^2$ for seventeenth century oak wood, which, considering a realistic spread in the material properties for oak wood, thus potentially may lead to crack formation comparable to that observed near cleated ends of seventeenth century historical cabinets displayed in museums, see Fig. 2. Alternatively, this value for the tensile stress may reach the strength of the glue connecting the oak wooden boards, thereby leading to failure of a glue joint.

As illustrated by the experimental deformations depicted in Fig. 9, the hygral shrinkage of the door panels tested appeared to occur predominantly in the horizontal direction. This supports the in-situ observation of Type 2 shrinkage cracks emerging *mainly* along the vertical direction of historical cabinet doors, see Fig. 2, i.e., perpendicular to the horizontal direction in which restrained hygral shrinkage leads to the development of significant tensile stresses in the panel substrate.

It must be emphasized that the basic bi-layer model sketched in Fig. 13 considers the stresses to be uniform in each layer, which provides an adequate estimate of the risk of climate-induced damage in a door panel if the spatial variations of stress within a layer are moderate too small. Essentially, the predictions following from Eq. (6) are useful for obtaining a first estimate of the risk of damage; a more detailed insight into this aspect requires the performance of advanced finite element analyses, in which climate-induced damage in oak wood panels is simulated by means of a coupled thermal–hygral–mechanical model that accounts for nucleation and propagation of discrete cracks. This type of analysis, however, falls beyond the scope of the present work, and is subject of future work.

Moisture content development

The time evolutions of the moisture content, measured at five different locations at the core of the boards of mockups A and B, are depicted in Fig. 17a and b, respectively. During the first 7 days of testing the relative humidity
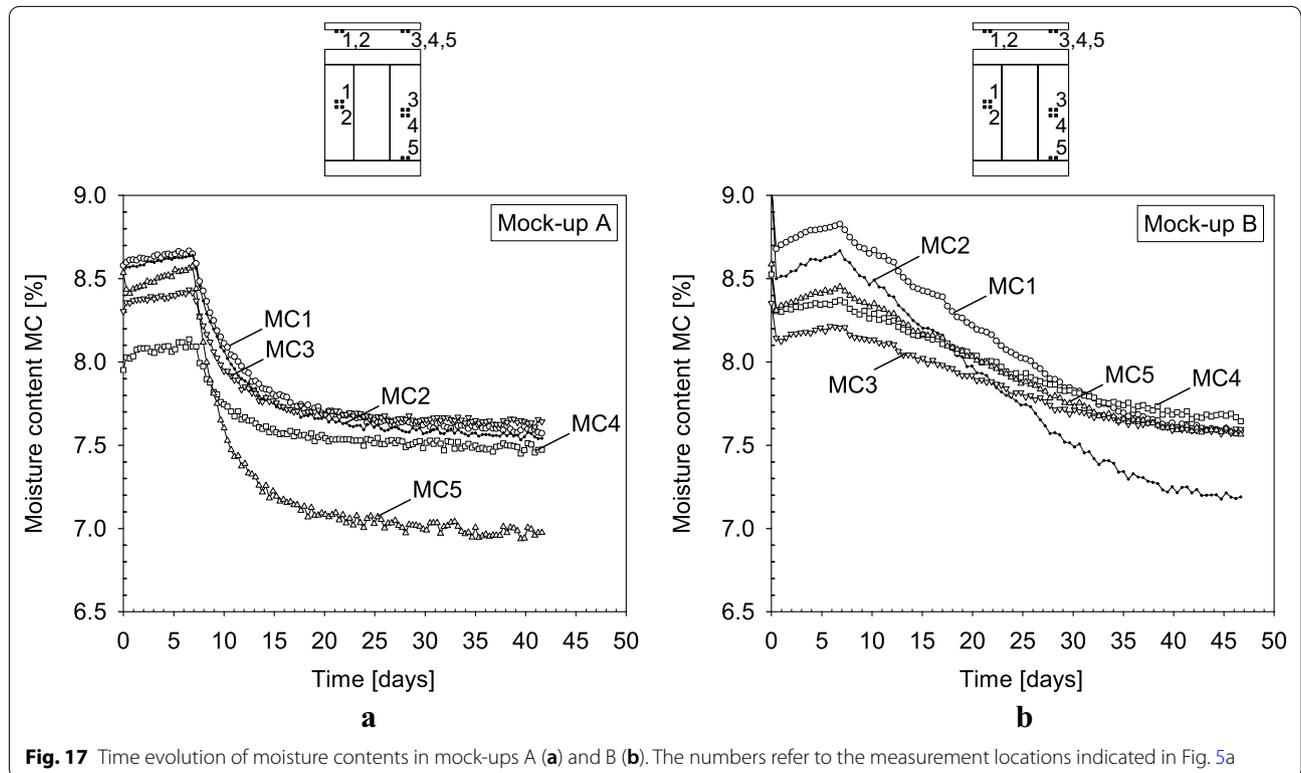

Fig. 17 Time evolution of moisture contents in mock-ups A (**a**) and B (**b**). The numbers refer to the measurement locations indicated in Fig. 5a

was kept constant, during which the moisture content only slightly varies in value, and for the five sensors lies in between 8.0 and 8.8%. Since it was confirmed that the relative humidity in the climate room was homogeneous, this spread in values is likely to be caused by spatial heterogeneities of the oak wood microstructure. After the initial stage, the relative humidity is lowered in an instantaneous (mock-up A) and stepwise (mock-up B) manner from 60 to 20%, as a result of which the moisture content in the panels decreases towards values between 6.9 and 7.7%.

The recorded decrease in moisture content can be compared to the values represented by the points A and B on the steady-state boundary curves depicted in Fig. 16. Sorption experiments were performed for the construction of these boundary curves and for the calibration of the depicted desorption scanning curve. The adsorption boundary curve provides an equilibrium moisture content of 8.9% at a relative humidity of 60%, see point A in Fig. 16, which lies somewhat above the range of initial moisture contents measured in the panels, see Fig. 17. Upon lowering the relative humidity towards 20%, the moisture content in Fig. 16 smoothly decreases along the desorption scanning curve towards an equilibrium moisture content of 5.1% on the desorption boundary curve, as indicated by point B in Fig. 16. It can be observed that this value lies approximately a factor of 1.5 below the range of final moisture contents recorded in the panels, see Fig. 17. The almost horizontal slopes observed at the end of the curves in Fig. 17 nevertheless suggest that these final moisture contents closely correspond to a steady state of hygroscopic equilibrium. The difference of a factor of 1.5 in equilibrium moisture content may be due to the reliability of the moisture sensors: unfortunately some inaccuracies caused by signal interference, signal instability and the influence of the electric current on the measured moisture content did appear during the testing procedure.

Experimental results mock-ups C, D, E and F
Deformation response
Mock-ups C to F were exposed to a relative humidity profile ranging between 35 and 71%, see Fig. 6c. Here, the configuration of mock-up D and F are the same as that of mock-ups A and B, while mock-ups C and E do not have cleated ends, and mock-ups E and F are constructed with veneer layers at the front and back sides of the substrate, see Fig. 3. The horizontal strain response measured at the half-length of the central board of mock-up D, as monitored by strain gauges SG6 and SG17, see Fig. 5b, is illustrated in Fig. 18, together with the relative humidity profile applied. It is observed that the signals recorded by the two strain gauges are virtually equal, and roughly follow the same trend as that of the relative humidity

profile applied. The maximal shrinkage strain at the half-length of the board is − 0.16%, which is 3 to 4 times lower than the maximum shrinkage strain of mock-up A under an instantaneous drop in relative humidity of 40%, see Fig. 7a.

In Fig. 19a–d the time evolution of the horizontal displacements recorded by the LVDTs sketched in the overview of Fig. 5b are depicted for mock-ups C, D, E and F, respectively. Clearly, the displacements develop along a similar trend as the strains depicted in Fig. 18. For mock-ups D and F the displacements of LVDT 1 and 5, measured near a cleated end across almost the complete width of the oak wood substrate, have a maximal value close to 0.6 mm, while for the mock-ups C and E without cleated ends this displacement approaches 1.2 mm. In other words, the presence of cleated ends locally reduces the horizontal deformation of the adjacent substrate by a factor of two. Further, the displacements recorded across an individual board (i.e., LVDT 2, 3, 4, 6, 7, 8) are one third to one half of the displacements recorded across the whole substrate (i.e., LVDT 1, 5), which is in correspondence with the substrate being constructed of three boards with some variation in width, see Table 1.

The time responses measured by the strain gauges other than SG6 and SG17 appear to follow a similar trend as those depicted in Fig. 18, and are not illustrated here for brevity. Instead, the time-averaged strains of the strain gauges ϵ_a, averaged per strain gauge group, are depicted in Fig. 20. For reasons of comparison, this is
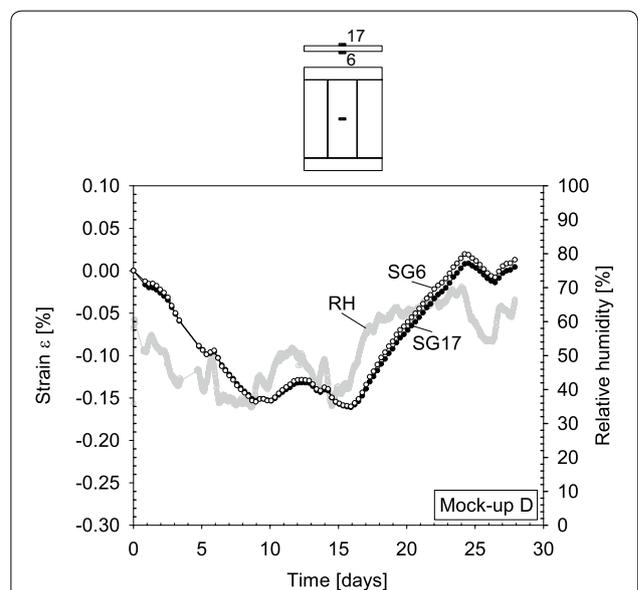

Fig. 18 Time evolution of horizontal strains in *mock-up D* for strain gauges 6,17 attached to the central board at the half-length of the panel, see Fig. 5b, together with the relative humidity profile imposed (taken from Fig. 6c)
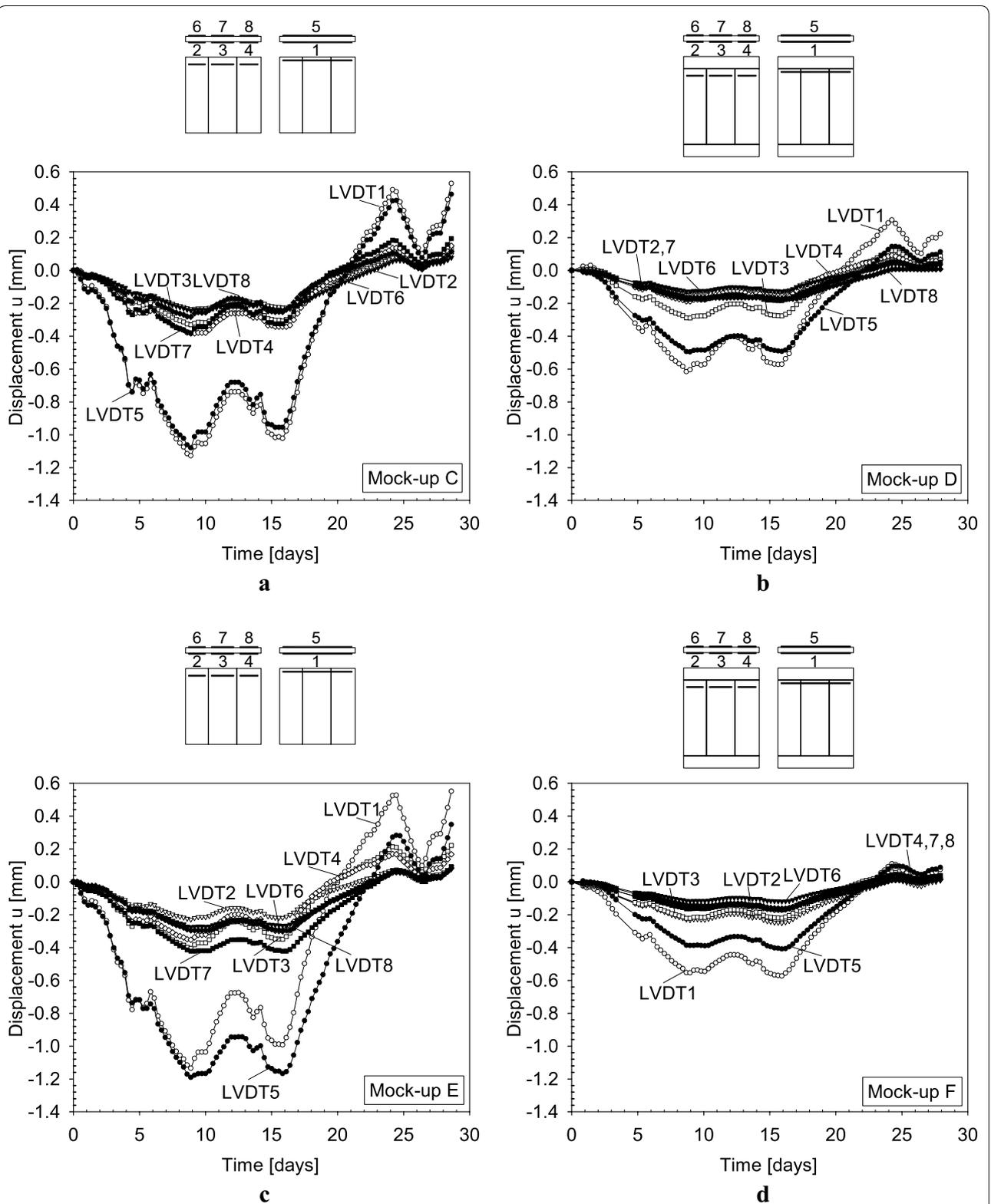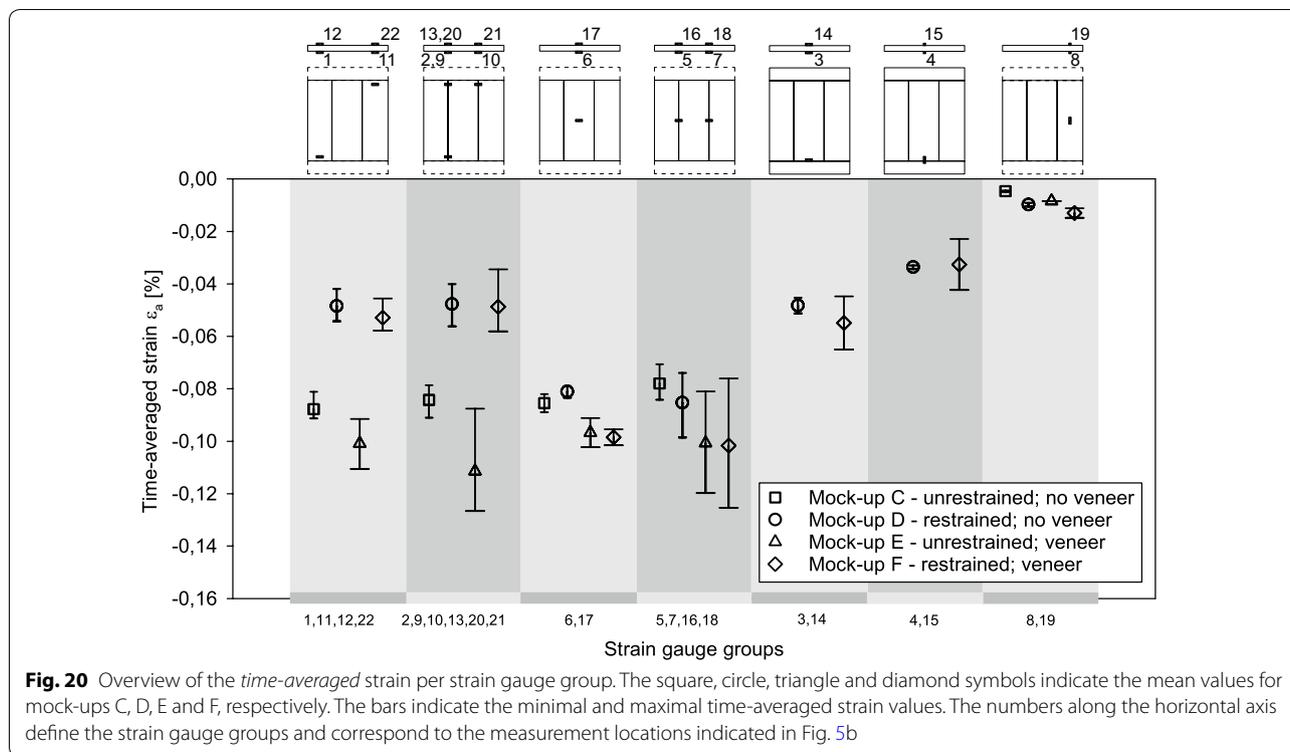
Luimes *et al. Herit Sci*   (2018) 6:72

Page 19 of 23

Fig. 19 Time evolution of displacements in mock-ups C (**a**), D (**b**), E (**c**) and F (**d**). The LVDT numbers refer to the measurement locations indicated in Fig. 5b

Luimes *et al. Herit Sci*   (2018) 6:72

Page 20 of 23

Fig. 20 Overview of the *time-averaged* strain per strain gauge group. The square, circle, triangle and diamond symbols indicate the mean values for mock-ups C, D, E and F, respectively. The bars indicate the minimal and maximal time-averaged strain values. The numbers along the horizontal axis define the strain gauge groups and correspond to the measurement locations indicated in Fig. 5b

done for all four mock-ups C, D, E and F. In accordance with the measurement scheme depicted in Fig. 5b, there are five strain gauge groups monitoring horizontal strains and two groups monitoring vertical strains.

Consistent with the results obtained for mock-ups A and B, for mock-ups D and F the horizontal shrinkage strain at the half-length of the panel (i.e., at strain gauge groups 6,17 and 5,7,16,18) is substantially larger—approximately a factor of two—than the horizontal shrinkage strain close to the cleated ends (i.e., at strain gauge groups 1,11,12,22, 2,9,10,13,20,21 and 3,14). In contrast, for mock-ups C and E without the cleated ends these strains are approximately equal, which again illustrates the restraining effect by the cleated end on local deformations in the panel. In addition, the horizontal shrinkage strains recorded at the centre of the panel are similar for the mock-ups with and without cleated ends, which confirms the earlier hypothesis that at the half-length of the panel the restraining effect by the cleated end on the deformation behaviour is negligible. It can be further noticed that the spread in strain values measured on mock-ups E and F with veneer layers is considerably larger than for mock-ups C and D without veneer layers. Hence, the addition of veneer layers increases the variability in the local deformation behaviour of a panel. On average, the horizontal shrinkage strains for the panels with veneer layers are slightly larger than those for

panels without veneer layers; this is caused by the fact that the hygroscopic expansion coefficient of the teak veneer layers in the tangential material direction (= horizontal panel direction) is larger than that of the oak substrate in the radial material direction (= horizontal panel direction). In accordance with the bi-layer model in Fig. 13 and Eq. (6), at the half-length of the panel this Type 2 shrinkage mechanism will induce a horizontal tensile stress in the veneer layer and a (small) horizontal compressive stress in the oak wood. This horizontal tensile stress indeed stimulates the development of vertical cracks in veneer layers, as regularly observed for historical cabinets [10]. These vertical cracks may subsequently deflect into delaminating cracks between the veneer layer and the substrate, with the chance of local spallation (i.e., flaking off) of the veneer layer. This failure mechanism is amplified by bending effects (warping) in the panel, see [30] for more details.

Since the spreads in strain values for the panels with and without veneer layers generally overlap, the influence by the veneer layers on the shrinkage behaviour of the substrate may be considered insignificant. This minor influence can be ascribed to the limited thickness of the veneer layers of 0.5 mm, see Table 1, which only represents 6% of the total panel thickness of 15.52 mm. It can be further seen that the strain values measured on an individual board are comparable to those measured

Luimes *et al. Herit Sci*   (2018) 6:72

Page 21 of 23

across the glue connection between two adjacent boards. This again confirms that the glue connections do not noticeably influence the local deformations of the oak wooden board. Finally, as also observed for mock-ups A and B, the recorded vertical strain values (i.e., at strain gauge groups 4,15 and 8,19) typically are smaller than the horizontal strain values, with the strain value measured at the centre of the panel being close to zero.

For brevity reasons, the final strain ϵ_f per strain gauge group, as depicted in Fig. 12 for mock-ups A and B, will not be shown for mock-ups C to F; this information appears to be comparable to that of the time-averaged strain depicted in Fig. 20, which may be ascribed to the smooth variations in the relative humidity profile imposed, see Fig. 6c.

Moisture content development

The development of the moisture content with time is illustrated in Fig. 21 at two different locations in mock-up D, together with the relative humidity profile imposed. The moisture sensors MC 1 and MC 2 are attached to a board at the half-length of the panel and near a cleated end, respectively, see Fig. 5b. Note that both moisture profiles start at a value relatively close to the equilibrium moisture content of 8.9%, as following from the adsorption boundary curve depicted in Fig. 16. The trends measured by the sensors clearly are comparable, and roughly follow the trend of the relative humidity profile applied. Note that the shortest fluctuations in relative humidity do not affect the moisture content profiles, which is due

Fig. 21 Time evolution of moisture content in mock-up D, together with the relative humidity profile imposed (taken from Fig. 6c). The numbers refer to the measurement locations indicated in Fig. 5b

to the characteristic minimal time it takes for the moisture to diffuse from the surface to the core of the board (which is where the sensors measure the signal). Since the moisture profiles for mock-ups C, E and F are similar to the profile of mock-up D, these are not illustrated here. Nonetheless, from this similarity it can be concluded that the presence of cleated ends and veneer layers does not significantly influence the moisture content development in the substrate.

Conclusions

The experimental study reported in this communication has led to several important insights and conclusions on the hygro-mechanical response of cabinet door panels under relative humidity fluctuations, which are summarized below. These conclusions provide a scientific basis for the understanding of shrinkage cracks and dimensional changes observed on decorated oak wooden panels in historical Dutch cabinets, and thus may assist in advising museums on future sustainable preservation strategies and rational guidelines for indoor climate specifications.

1. *Restrained hygral shrinkage* observed in cabinet door panels can be a source of damage formation. As demonstrated by means of a hygro-mechanical bi-layer model, this shrinkage may originate from: (i) a difference in moisture content across the thickness direction of the panel, referred to as *Type 1* shrinkage, or (ii) a directional difference in the coefficients of hygroscopic expansion of structural components forming a coherent connection, referred to as *Type 2* shrinkage. Type 1 shrinkage occurs in the outer regions of the panel thickness, whereas Type 2 shrinkage takes place at the cleated ends of a panel.

2. Under a maximally applied decrease in relative humidity of 40%, the panels tested did not show any shrinkage cracking in the oak wood or the glue connections, no matter whether this decrease in relative humidity was applied abruptly or in a more gradual, step-wise fashion. By means of a basic analytical bi-layer model it has been demonstrated that the local tensile stresses developing in the panels under restrained hygral shrinkage indeed were lower than the tensile strength of new oak wood perpendicular to the grain direction, as reported recently in [28]. Nonetheless, the tensile stress generated near the cleated end—as a result of Type 2 shrinkage—is comparable to the tensile strength of seventeenth century oak wood reported in [28], which possibly explains the crack formation regularly observed near cleated ends in seventeenth century historical cabinets, see Fig. 2. Alternatively, these cracks may result from the local tensile stress reaching the fracture strength of the (aging) historic glue connecting the oak wooden boards, leading to failure of a glue joint.
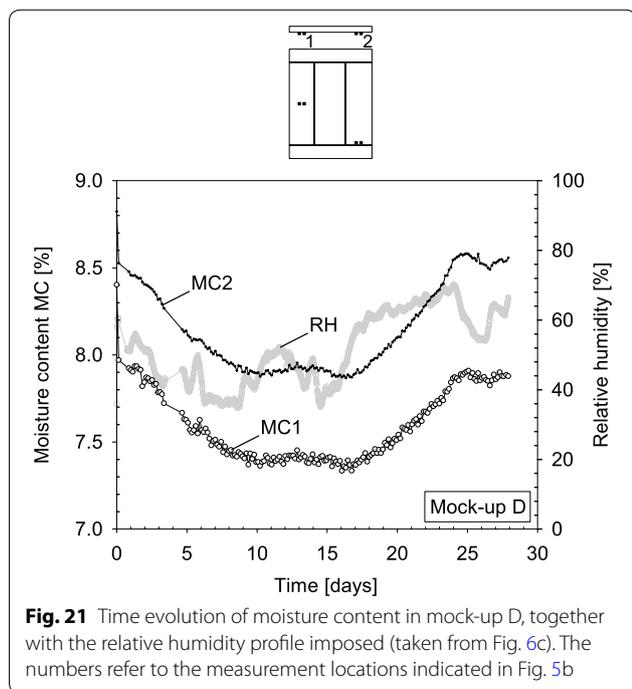
Luimes *et al. Herit Sci*   (2018) 6:72

Page 22 of 23

3. The presence of *cleated ends* locally reduces the horizontal (Type 2) shrinkage of the substrate by approximately a factor of two, regardless of the features of the humidity profile applied. Together with the above conclusions (1) and (2), this experimental result supports the observation from the museum study reported in [25] that historical door panels *with* and *without* cleated ends respectively show the *most* and *least* damage.

4. The presence of teak *veneer layers* induces a Type 2 shrinkage mechanism via its connection to the oak wood substrate below. At the half-length of the panel this leads to a horizontal tensile stress developing in the veneer layer and a (small) horizontal compressive stress evolving in the oak wood. This horizontal tensile stress indeed stimulates the development of vertical cracks in veneer layers, as regularly observed for historical cabinets [10].

5. The hygral shrinkage of the mock-ups tested predominantly occurred in the horizontal direction. This supports the in-situ observation of Type 2 shrinkage cracks emerging *mainly* in the vertical direction of historical cabinet doors, see Fig. 2, i.e., perpendicular to the horizontal direction in which restrained hygral shrinkage may induce significant tensile stresses in the panel substrate.

6. A few mock-ups experienced some warping under the relative humidity variations applied. This is caused by the fact that the boards composing the panel substrate were not always ideally quarter-sawn, which resulted in different amounts of shrinkage at the back and front sides of the board. This may explain the warping observed in door panels of seventeenth century cabinets displayed in museums [10].

As a final note, it is mentioned that a detailed study of the damage generated by restrained hygral shrinkage in oak wooden panels requires the performance of advanced finite element analyses, in which a coupled thermal–hygral–mechanical modelling approach is used that accounts for the nucleation and propagation of discrete cracks. This type of analysis, however, falls beyond the scope of the present work, and will be presented in a forthcoming publication.

Authors' contributions
RAL set up the experimental program, executed the experiments and drafted the manuscript. ASJS assisted in setting up the experimental program, derived the analytical bi-layer model on restrained hygral shrinkage, and drafted the manuscript. AJMJ assisted in setting up the experimental program and reviewed the manuscript. PHJCD assisted in setting up the experimental program and reviewed the manuscript. HLS assisted in setting up the experimental program and reviewed the manuscript. All authors read and approved the final manuscript.

Author details
[1] Department of the Built Environment, Eindhoven University of Technology, P.O. Box 513, 5600 MB Eindhoven, The Netherlands. [2] Department of Conservation and Scientific Research, Rijksmuseum Amsterdam, Hobbemastraat 22, 1071 ZC Amsterdam, The Netherlands.

Publisher's Note
Springer Nature remains neutral with regard to jurisdictional claims in published maps and institutional affiliations.

References
1. Boersma F, Dardes K, Druzik J. Precaution, proof, and pragmatism. Evolving perspectives on the museum environment. In: Conservation perspectives. The GCI newsletter. Collection Environments. The Getty Conservation Institute; 2014. p. 4–9.
2. Luciani A. Historical climates and conservation environments. Historical perspectives on climate control strategies within museums and heritage buildings [Dissertation]. Politecnico di Milano; 2013.
3. Bickersteth J. Environmental conditions for the safeguarding of collections: what should our set points be? Stud Conserv. 2014;59(4):218–24.
4. Bickersteth J. IIC and ICOM-CC 2014 declaration on environmental guidelines. Stud Conserv. 2016;61(sup1):12–7.
5. Kirby Atkinson J. Environmental conditions for the safeguarding of collections: a background to the current debate on the control of relative humidity and temperature. Stud Conserv. 2014;59(4):205–12.
6. Staniforth S. Environmental conditions for the safeguarding of collections: future trends. Stud Conserv. 2014;59(4):213–7.
7. Michalski S. The ideal climate, risk management, the ASHRAE chapter, proofed fluctuations, and toward a full risk analysis model. In: Boersma F, editor. Contribution to the experts roundtable on sustainable climate management strategies. Tenerife: The Getty Conservation Institute; 2007. p. 1–19.
8. Erhardt D, Tumosa CS, Mecklenburg MF. Applying science to the question of museum climate. In: Padfield T, Borchersen K, editors. Museum microclimates. Copenhagen: The National Museum of Denmark; 2007. p. 11–8.
9. van Duin P. Climate effects on museum objects. The need for monitoring and analysis. In: Conservation perspectives. The GCI newsletter. Collection Environments. The Getty Conservation Institute; 2014. p. 13–15.
10. van Duin PHJC. The construction of flat decorated doors of Dutch seventeenth-century cabinets, report of a master class. In: Vasques Dias M, editor. Restoring joints, conserving structures. Amsterdam: Stichting Ebenist; 2010. p. 121–43.
11. van Gerven G, Ankersmit B, van Duin PHJC, Jorissen AJM, Schellen HL. A controlled method to flatten warped wooden panels. Stud Conserv. 2016;61(3):125–35.
12. Huijbregts Z, Schellen H, van Schijndel J, Ankersmit B. Modelling of heat and moisture induced strain to assess the impact of present and

Luimes *et al. Herit Sci*   (2018) 6:72

Page 23 of 23

historical indoor climate conditions on mechanical degradation of a wooden cabinet. J Cult Herit. 2015;16:419–27.

13. Saft S, Kaliske M. Computational approach towards structural investigations for the restoration of historical keyboard instruments. J Cult Herit. 2012;13S(3):S165–74.

14. Goli G, Dionisi-Vici P, Uzielli L. Locating contact areas and estimating contact forces between the "Mona Lisa" wooden panel and its frame. J Cult Herit. 2014;15:391–402.

15. Bratasz L, Kozlowski R, Camuffo D, Pagan E. Impact of indoor heating on painted wood—monitoring the altarpiece in the church of Santa Maria Maddalena in Rocca Pietore, Italy. Stud Conserv. 2007;52(3):199–210.

16. Rachwal B, Bratasz L, Krzemień M, Lukomski M, Kozlowski R. Fatigue damage of the gesso layer in panel paintings subjected to changing climate conditions. Strain. 2012;48:474–81.

17. Rachwal B, Bratasz L, Lukomski M, Kozlowski R. Response of wood supports in panel paintings subjected to changing climate conditions. Strain. 2012;48:366–74.

18. Lukomski M. Painted wood. What makes the paint crack? J Cult Herit. 2012;13S:S90–3.

19. Dionisi-Vici P, Mazzanti P, Uzielli L. Mechanical response of wooden boards subjected to humidity step variations: climate chamber measurements and fitted mathematical models. J Cult Herit. 2006;7:37–48.

20. van Grevenstein A, New B, Young C, Seymour K, Groves R, Horie V. The conservation of panel paintings and related objects. In: van Duin P, editor. Research agenda 2014–2020. The Hague: The Netherlands Organisation for Scientific Research in association with Rijksmuseum Amsterdam; 2014.

21. The Getty Conservation Institute. Managing Collection Environments Initiative; 2018. http://www.getty.edu/conservation/our_projects/education/managing/index.html. Accessed Sept 2018.

22. Schellen HL, van Duin PHJC, Ekelund SE, Luimes RA, Gauvin CAF, Jorissen AJM, et al. Climate4Wood: climate effects on decorated wooden panels. In: NWO Science4Arts Symposium. Amsterdam, The Netherlands: Netherlands Organisation for Scientific Research; 2016. p. 13–17.

23. Ekelund S, van Duin P, Jorissen A, Ankersmit B, Groves RM. A method for studying climate-related changes in the condition of decorated wooden panels. Stud Conserv. 2018;63(2):62–71.

24. Druzik J. Epidemiology applied to museum collections. In: Druzik J, Boersma F, editors. Epidemiology: basic ideas applied to museum collections. Log Angeles: The Getty Conservation Institute; 2015. p. 5–25.

25. Ekelund SE, Jorissen AJM. The Museum Study of the Climate4Wood research project. In: Jorissen AJM, Leijten AJM, editors. Proceedings of Research symposium: Structural Design with Timber. ISBN 978-90-386-3562-0. Eindhoven: Eindhoven University of Technology; 2014. p. 93–109.

26. CEN. EN 16682: Conservation of cultural heritage—methods of measurement of moisture content, or water content, in materials constituting immovable cultural heritage; 2017.

27. Saft S, Kaliske M. A hybrid interface-element for the simulation of moisture-induced cracks in wood. Eng Fract Mech. 2013;102:32–50.

28. Luimes RA, Suiker ASJ, Verhoosel CV, Jorissen AJM, Schellen HL. Fracture behaviour of historic and new oak wood. Wood Sci Technol. 2018;52:1243–69.

29. Frandsen HL, Svensson S, Damkilde L. A hysteresis model suitable for numerical simulation of moisture content in wood. Holzforschung. 2007;61(2):175–81.

30. Forschelen PJJ, Suiker ASJ, van der Sluis O. Effect of residual stress on the delamination response of film-substrate systems under bending. Int J Solids Struct. 2016;97–98:284–99.